Quaternary Science Reviews
September 2015, Volume 123 Pages 113-133
http://dx.doi.org/10.1016/j.quascirev.2015.06.010
http://archimer.ifremer.fr/doc/00272/38346/
© 2015 Elsevier Ltd. All rights reserved.

Achimer
http://archimer.ifremer.fr

Millennial-scale fluctuations of the European Ice Sheet at the end of the last glacial, and their potential impact on global climate

Toucanne Samuel [1,*], Soulet Guillaume [2], Freslon Nicolas [1], Silva Jacinto Ricardo [1], Dennielou Bernard [1], Zaragosi Sébastien [3], Eynaud Frédérique [3], Bourillet Jean-Francois [1], Bayon Germain [1]

[1] Institut Français de Recherche pour l'Exploitation de la Mer (IFREMER), Unité de Recherche Géosciences Marines, F-29280 Plouzané, France
[2] Woods Hole Oceanographic Institution (WHOI), Department of Geology and Geophysics, MA 02543, USA
[3] Université de Bordeaux, UMR-CNRS 5805 EPOC, F-33405 Talence, France

Corresponding author : Samuel Toucanne, email address : stoucann@ifremer.fr

Abstract :

Reconstructing Northern Hemisphere ice-sheet oscillations and meltwater routing to the ocean is important to better understand the mechanisms behind abrupt climate changes. To date, research efforts have mainly focused on the North American (Laurentide) ice-sheets (LIS), leaving the potential role of the European Ice Sheet (EIS), and of the Scandinavian ice-sheet (SIS) in particular, largely unexplored. Using neodymium isotopes in detrital sediments deposited off the Channel River, we provide a continuous and well-dated record for the evolution of the EIS southern margin through the end of the last glacial period and during the deglaciation. Our results reveal that the evolution of EIS margins was accompanied with substantial ice recession (especially of the SIS) and simultaneous release of meltwater to the North Atlantic. These events occurred both in the course of the EIS to its LGM position (i.e., during Heinrich Stadial –HS– 3 and HS2; ~31–29 ka and ~26–23 ka, respectively) and during the deglaciation (i.e., at ~22 ka, ~20–19 ka and from 18.2 ± 0.2 to 16.7 ± 0.2 ka that corresponds to the first part of HS1). The deglaciation was discontinuous in character, and similar in timing to that of the southern LIS margin, with moderate ice-sheet retreat (from 22.5 ± 0.2 ka in the Baltic lowlands) as soon as the northern summer insolation increase (from ~23 ka) and an acceleration of the margin retreat thereafter (from ~20 ka). Importantly, our results show that EIS retreat events and release of meltwater to the North Atlantic during the deglaciation coincide with AMOC destabilisation and interhemispheric climate changes. They thus suggest that the EIS, together with the LIS, could have played a critical role in the climatic reorganization that accompanied the last deglaciation. Finally, our data suggest that meltwater discharges to the North Atlantic produced by large-scale recession of continental parts of Northern Hemisphere ice sheets during HS, could have been a possible source for the oceanic perturbations (i.e., AMOC shutdown) responsible for the marine-based ice stream purge cycle, or so-called HE's, that punctuate the last glacial period.

Please note that this is an author-produced PDF of an article accepted for publication following peer review. The definitive publisher-authenticated version is available on the publisher Web site.

Keywords : European ice-sheet, Channel River, Meltwater, Deglaciation, Neodymium, Termination

Highlights

► Nd isotope evidence for sources of Channel River meltwater discharges. ► Meltwater discharges caused by recession of the EIS into the North European Plain. ► Timing of runoff pulses provide new insights into EIS history. ► Temporal match between runoff pulses and AMOC shutdown reveals the role of the EIS in past global climate changes.

Please note that this is an author-produced PDF of an article accepted for publication following peer review. The definitive publisher-authenticated version is available on the publisher Web site.

1. INTRODUCTION

A central question of climate sciences is the understanding of the causes of the Pleistocene ice ages, and of the rapid collapse of ice-sheets (i.e., 'terminations'; see Paillard, 2015 for a thorough review). The emergent 'termination paradigm' posits that the necessary condition to drive the earth out of ice ages is the occurrence of a single (Terminations II and IV) or series (Terminations I and III) of multi-millennial climatic oscillations involving variations in the strength of Atlantic Meridional Oceanic Circulation (AMOC) (Barker et al., 2011; Broecker et al., 2010; Cheng et al., 2009; Denton et al., 2010; Ruddiman et al., 1980). These long-lived AMOC slowdowns would have led to prolonged stadial conditions in the Northern Hemisphere (NH), Southern Hemisphere (SH) warming, and CO_2 degassing from the Southern Ocean, in turn amplifying global deglacial warming (Barker et al., 2009; Cheng et al., 2009; Denton et al., 2010; Shakun et al., 2012). Thus, the 'termination paradigm' implies that the primary condition required to trigger a termination is not solely the magnitude of the boreal insolation change but also a sufficient volume of freshwater released into the North Atlantic that can perennially weaken the AMOC. The only available reservoir for such large volumes of fresh water was the extensive and isostatically-depressed Laurentide (LIS) and European (EIS) ice-sheets that achieved maxima on both sides of the North Atlantic at the end of each ice age. However, the potential sources of such prolonged events of freshwater release and any associated AMOC reduction are still uncertain due to the difficulties to connect continental ice-sheet fluctuations and associated meltwater releases to paleoclimatic and paleoceanographic records (e.g., Broecker, 2006). In the specific case of the last Termination (~19 to 10 ka; Clark et al., 2012c), the first prolonged event of AMOC reduction is thought to have occurred between ~18 and 15 ka (Hall et al., 2006; McManus et al., 2004), corresponding to Heinrich Stadial 1 (HS1). Evidence from the southern LIS margin and the western North Atlantic suggest that the LIS could have provided substantial freshwater during this interval (Clark et al., 2004a; Clark et al., 2007; Clark et al., 2001), as well as during the subsequent prolonged AMOC slowdown that occurred during the Younger Dryas cold event (Broecker et al., 1988; Carlson et al., 2007; Clark et al., 2004a; Clark et al., 2007; Clark et al., 2001). The meltwater contribution of the EIS remains largely unknown in comparison. Substantial hydrographic changes have been reported along the European margin at times of AMOC perturbations including HS1, thus pointing out the possible participation of the EIS to these events (Eynaud et al., 2012; Hall et al., 2011; Hall et al., 2006; Knutz et al., 2007; Lekens et al., 2006; McCabe and Clark, 1998; Peck et al., 2006; Peck et al., 2007; Scourse et al., 2000). However, our understanding remains incomplete since the correlation of EIS fluctuations with these paleoceanographic changes and with well-dated proxy records for AMOC variability only relate to the marine ice-streams and ice-shelves draining into the North Atlantic (e.g., Peck et al., 2006). In contrast, the correlation with the evolution of the major terrestrial ice-streams in the southern EIS (e.g., southern Baltic ice stream complex), known to be very active due to melting bed conditions (Boulton et al., 2001; Boulton et al., 1985), is poorly documented (Lehman et al., 1991; Rinterknecht et al., 2006). In addition, hosing experiments demonstrate that the sensitivity of ocean circulation depends on the location of the freshwater perturbation and that the climate system is very sensitive to freshwater perturbations originating from the European margin (Roche et al., 2010). Finally, just as the LIS, the EIS had reached its maximum extent during the Last Glacial Maximum (LGM, ~26-19 ka; Clark et al., 2009), making it a potential source of freshwater at the end of the last ice age. This leads to the possibility that the EIS might have played a significant role in the first steps of the last termination.

The EIS, composed of the British-Irish (BIIS) and the Scandinavian (SIS) ice sheets, formed the second largest NH ice mass (Fig. 1). The two regional ice-sheets merged during the last glacial (Bradwell et al., 2008; Carr et al., 2000; Sejrup et al., 2009), covering the North Sea area and leading to the formation of a large river system that drained the western European continent (Gibbard, 1988; Toucanne et al., 2009b; Toucanne et al., 2010). During glacial times, the so-called Channel River routed substantial amounts of meltwater to the North Atlantic (Eynaud et al., 2007; Ménot et al., 2006; Roche et al., 2010; Toucanne et al., 2010; Zaragosi et al., 2001). To explore the potential role of the EIS during the last termination, we investigate the link between the EIS ice-margin fluctuations, Channel River meltwater discharge, and AMOC rate. Our results provides direct evidence that the EIS played a crucial role in the abrupt reorganizations of the global climate system that accompanied the end of the last glacial period.

2. MATERIAL AND METHODS

We focus on core MD95-2002, a sedimentary archive recovered directly off the mouth of the Channel River (Meriadzek Terrace; 2,174 m water depth; 47'27°N, 8'32°W) (Fig. 1). Previous studies have shown that core MD95-2002 is suitable for reconstructing the deglacial pulses of meltwater emanating from the EIS (Eynaud et al., 2012; Eynaud et al., 2007; Ménot et al., 2006; Toucanne et al., 2009a; Toucanne et al., 2010; Zaragosi et al., 2001). To decipher the coupling between EIS ice-margin fluctuations and Channel River meltwater discharge, we measured Nd isotope ratios of fine-grained detrital fraction from this core (n=95). The neodymium isotopic composition (ε_{Nd}) of terrigenous sediment is a powerful tracer for geographical provenance because the ε_{Nd} signature of detrital sediment is retained during continental weathering and subsequent transport (Goldstein and Jacobsen, 1988). Considering that clays and silts are the dominant size-fractions transported to the sea by meltwaters emanating from ice-margins (e.g. Brown and Kennett, 1998), we focused our analyses on the clay-silt fraction (<63µm) of the MD95-2002 samples. In order to link the observed ε_{Nd} changes to potential source regions, a series of 45 LGM glacigenic samples from moraines, ice-marginal valleys and proglacial lakes alongside the EIS southern margin and a suite of 33 modern sediments recovered from the mouth (i.e., mudflats, delta, bays, lagoons) of various European rivers were analysed (Fig. 1), focusing on the clay-silt fraction for comparison with the MD95-2002 samples. Fine-grained river sediments integrate the geochemical diversity of catchment areas, and as such can provide a reliable average Nd isotopic composition of their corresponding drainage basin (Goldstein and Jacobsen, 1988).

Dried fine-grained fractions (typically ~ 0.5 g) were crushed using an agate mortar and pestle. The terrigenous fraction of each sediment sample was digested by alkaline fusion (Bayon et al., 2009) after removal of all carbonate, Fe-Mn oxyde and organic components using a sequential leaching procedure (Bayon et al., 2002). Prior to analyses, the Nd fractions were isolated by ion chromatography (see details in Bayon et al., 2012). Isotopic measurements were performed at the Pôle Spectrométrie Océan, Brest (France), using a Thermo Scientific Neptune multi-collector ICPMS. Mass bias corrections on Nd were made with the exponential law, using $^{146}Nd/^{144}Nd = 0.7219$. Nd isotopic compositions were determined using sample-standard bracketing, by analysing JNdi-1 standard solutions every two samples. Mass-bias corrected values for $^{143}Nd/^{144}Nd$ were normalized to a JNdi-1 value of $^{143}Nd/^{144}Nd = 0.512115$ (Tanaka et al., 2000). Replicate analyses of the JNdi-1 standard solution during the course of this study gave $^{143}Nd/^{144}Nd = 0.512095 \pm 0.000009$ (2SD, $n = 150$), which corresponds to an external reproducibility of ~ ±0.3 ε-units, taken as the estimated uncertainty on our measurements. In this study, both measured $^{143}Nd/^{144}Nd$ ratios and literature data are reported in ε_{Nd} notation, $[(^{143}Nd/^{144}Nd)_{sample}/(^{143}Nd/^{144}Nd)_{CHUR} - 1] \times 10^4$, using $(^{143}Nd/^{144}Nd)_{CHUR} = 0.512638$ (Jacobsen and Wasserburg, 1980).

Finally, the bulk intensity of major elements for core MD95-2002 was analyzed using an Avaatech X-Ray Fluorescence (XRF) core scanner at the Institut Français de Recherche pour l'Exploitation de la Mer (IFREMER), Brest (France). XRF data were measured every 10mm along the entire length of the core, with a count time of 10 seconds, by setting the voltage to 10 kV (no filter) and 30 kV (Pd thick filter) and the intensity to 600 mA and 1000 mA, respectively. The same methodology was used to analyse the bulk intensity of major elements of cores MD03-2690 and MD03-2695 (Armorican turbidite system; Toucanne et al., 2008) (see Fig. 1 for location). Only data for Titanium (Ti), Iron (Fe) and Calcium (Ca) are reported in this study. It is commonly assumed that Ti and Fe elements are related to terrigenous-siliciclastic components (clays, heavy minerals), while Ca mainly reflects the marine carbonate content (calcite and aragonite) in the sediment (Richter et al., 2006). Therefore the ratios of XRF intensities of Ti and Ca (Ti/Ca) and Fe and Ca (Fe/Ca) were previously used to estimate terrigenous inputs on continental margins, and by extension past river runoff (e.g., Arz et al., 1998; Jennerjahn et al., 2004; Toucanne et al., 2009a; Ziegler et al., 2013).

3. MD95-2002 CORE CHRONOLOGY

The chronostratigraphic framework of core MD95-2002 is based on 22 monospecific ^{14}C ages [performed on *Globigerina bulloides* and *Neogloboquadrina pachyderma* (left coiling) from the >150µm fraction] and 4 additional ^{14}C ages from nearby cores MD03-2692 (Trevelyan Escarpment; Eynaud et al., 2007; Mojtahid et al., 2005) and MD03-2690 (Armorican turbidite system; Toucanne et al., 2008) (Figs 2, 3 and 4; Table 1). The cores were synchronized by means of their XRF-Ti/Ca records with an estimated error of less than 10 cm (Fig. 2). Additional control-points were added to the age model by tuning the *N. pachyderma* abundance to the NGRIP ice core $\delta^{18}O$ record (GICC05 timescale; Andersen et al., 2006)

(Table 1). To do so, we assumed that abrupt changes in the *N. pachyderma* abundance (interpreted as latitudinal migration of the polar front) were coeval to the sharp changes in Greenland air temperature (Bond et al., 1993; Eynaud et al., 2012; Scourse et al., 2009; Zaragosi et al., 2001). ^{14}C ages were first corrected for reservoir age and then calibrated to calendar age using the IntCal13 calibration curve (Reimer et al., 2013). The current regional reservoir age is 352 ± 92 ^{14}C years (average of the reservoir ages reported for the 100 locations closest to MD95-2002 site; http://www.calib.qub.ac.uk/marine). However, the regional reservoir age has changed through time (Stern and Lisiecki, 2013). Prior to HS1 and during the Holocene, reservoir age was almost constant and centred on ~400 ± 200 ^{14}C years. During HS1, the Bølling-Allerød (BA) and the Younger Dryas, average reservoir ages were 970, 680 and 875 ^{14}C years with a typical uncertainty of 200 ^{14}C years (1σ). All these climatic events are easily identifiable owing to MD95-2002 left coiling *N. pachyderma* stratigraphy (Eynaud et al., 2012; Zaragosi et al., 2001). Thus, ^{14}C ages from each stratigraphic unit were corrected for the *ad hoc* reservoir age and uncertainty was propagated through the quadratic sum (Table 1). The comparison of NGRIP and the *N. pachyderma* stratigraphy at the HS1/BA transition illustrates the suitability of the applied reservoir correction. Indeed, the abrupt decrease in *N. pachyderma* abundance between 380 cm [13,020 ± 60 ^{14}C years before present (BP); Table 1] and 390 cm (13,170 ± 70 ^{14}C years BP) in MD95-2002 corresponds to the BA NGRIP's sharp increase in air temperature dated to 14,640 ± 90 calendar years BP (Andersen et al., 2006). This corresponds to 12,460 ± 40 ^{14}C years BP according to the IntCal13 calibration curve. This leads to reservoir ages of 560 ± 70 and 710 ± 80 ^{14}C years for depths 380 and 390 cm, respectively. These values are statistically indistinguishable from the 680 ± 200 ^{14}C years (Stern and Lisiecki, 2013) reservoir correction applied. The final age model was performed using the age modelling software Clam (Blaauw, 2010; version 2.2) and reported with 95% confidence intervals (Fig. 3). The additional control-points obtained from the *N.*

pachyderma - $\delta^{18}O$ NGRIP tuning are shown in Fig. 5 along with the core ε_{Nd} and XRF-Ti/Ca records. Note that the deglacial chronology in the Baltic lowlands (i.e., R3, R4 and R5 events, see below) is entirely independent of ice-core age models since it is only based on ^{14}C ages (Fig. 4 and Table 1).

4. GEOCHEMICAL RESULTS

4.1 X-RAY FLUORESCENCE

The XRF Ti/Ca and Fe/Ca ratios in core MD95-2002 show a good correlation ($r = 0.975$; $p < 0.01$) all along the sedimentary sequence (Figs 4 and 5), indicating that the Fe and Ti elements fluctuate together from a common source. Higher (lower) values of both ratios are observed during stadials (interstadials), when sedimentation rates in core MD95-2002 (Fig. 3) and turbidite flux in the deep Bay of Biscay (Toucanne et al., 2012; Toucanne et al., 2008) reach high (low) levels (Figs 4 and 5). Taken collectively, the data suggest that the Fe and Ti elements are related to terrigenous-siliciclastic components and the carbonate content in the core is mainly due to dilution by terrigenous sediment. Thus, the Ti/Ca and Fe/Ca can be used as a first-order indication of relative changes in the amount of fine terrigenous components supplied to the core site from Channel River discharge. However, this interpretation is not tenable for the millennial-scale minima in Ti/Ca and Fe/Ca observed at ca. 24 ka (second part of HS2) and ca. 16 ka (second part of HS1) since anaerobic microbial decomposition of organic matter during these ~300-years intervals led to bicarbonate supersaturation and precipitation of calcite at site MD95-2002 (Auffret et al., 1996; Toucanne, 2008). These layers, also characterised by abundant ice-rafted debris (IRD; Auffret et al., 2002; Grousset et al., 2000), probably correspond to the 'cemented marls' of Hemming et al. (2004) which they interpreted as discharge of icebergs from the Hudson Strait Ice Stream of the LIS to the North Atlantic (i.e., so-called Heinrich Events -HE- that are part of the HS).

4.2 ND ISOTOPES

4.2.1 Modern rivers

The Nd isotopic compositions of the European river sediments analysed in this study (*n* = 33) range from ε_{Nd} values of -23.3 (Kiiminkijoki River) to -6.7 (Thames River) (Fig. 6 and Table 2). To a large extent, the distribution of Nd isotopic ratios in European river sediments is controlled by the lithological diversity and the age of the source rocks (Goldstein and Jacobsen, 1987; Goldstein et al., 1984; Peucker-Ehrenbrink et al., 2010). Indeed, very unradiogenic values ($-23.3 < \varepsilon_{Nd} < -13.8$) characterise rivers draining the Precambrian Baltic Shield (i.e., Scandinavia), which is known as one of the oldest geological formations in Europe (Bogdanova et al., 2008). In contrast, the Nd isotopic signature of the sediment carried by the rivers draining the Baltic (i.e., Narva, Gauja, Daugava, Neman and Vistula rivers), Paris (e.g., Authie, Orne, Seine, Somme rivers) and London (e.g., Colne, Hamble, Thames rivers) sedimentary basins of Phanerozoic age show more radiogenic values ($-16.4 < \varepsilon_{Nd} < -6.7$). This is well-expressed for the western part of the British Isles ($\varepsilon_{Nd} = -10.8 \pm 1.0$) when focusing on the weighted mean ε_{Nd} signature (considering the river drainage surface) for the different European regions (Table 2). Such a signature is inherited from the recycling of crust material derived from former orogeny events, such as the Caledonian and Variscan orogens for the western European continent and the southern British Isles (Davies et al., 1985; Michard et al., 1985). Similarly, the filling of the Baltic Basin (i.e., eastern part of the North European Plain; Fig. 1) mainly derived from the erosion of the Baltic Shield (Ūsaityte, 2000), thus explaining the unradiogenic character (i.e., in comparison to that of the western British

Isles) of the Nd isotopic signature ($-16.4 < \varepsilon_{Nd} < -14.3$) of river sediments from Poland and the Baltic States (Table 2).

4.2.2 LGM glacigenic sediments

The Nd isotopic compositions of the LGM glacigenic sediment (n = 45) collected alongside the EIS southern margin (i.e., Ireland, UK, North Sea, Denmark, Germany and Poland; see Table 3 and associated references for details about their stratigraphy) range from ε_{Nd} values of -16.8 (Lønstrup Klint Fm, Denmark) to -0.6 (Kilmore Quay, Ireland) (Fig. 6 and Table 3). With the exception of the very unradiogenic Irish sample from Kilmore Quay (most likely due to its proximity to local Ordovician volcanic rocks), the Nd isotopic data of the LGM glacigenic sediment resemble that observed for modern rivers at the European scale, with a general decrease from West ($\varepsilon_{Nd} = -11.8 \pm 0.7$ in Ireland; Kilmore Quay sample excluded) to East ($\varepsilon_{Nd} = -15.0 \pm 1.1$ in the North European Plain, Table 3). This indicates that the BIIS and the Irish Sea Ice Stream (ISIS) mobilised more radiogenic sediment that the SIS during the LGM. Interestingly, the Nd isotopic compositions of the LGM glacigenic sediment collected in Denmark ($-16.8 < \varepsilon_{Nd} < -13.0$) and Germany ($-16.5 < \varepsilon_{Nd} < -12.4$) significantly differ from that encountered in modern river sediments in this region ($-12.4 < \varepsilon_{Nd} < -8.9$, see Table 2). This leads to an homogeneous, low ε_{Nd} signature of glacigenic material along the southern SIS, from Baltic States to Denmark. This probably highlights both the input of Baltic Shield materials in the North European Plain by the southern SIS margins (Kjær et al., 2003), and the westward transport of sediment from Poland and the Baltic States (see the Neodymium isotope signature for modern rivers in Table 2) in continuous, extensive ice-marginal valleys (Ehlers et al., 2011a; Krzyszkowski et al., 1999) (Figs 1 and 6).

4.2.3 MD95-2002 ε_{Nd} record

The new MD95-2002 ε_{Nd} record shows significant fluctuations over the studied interval (Figs 4 and 5; Supplementary Material for numeric data). While Nd isotope data are stable around ε_{Nd} value of -11.5 before 32 ka and after 11 ka, the Nd isotope data largely fluctuate over the 32-11 ka interval with ε_{Nd} values ranging from -14.2 to -9.7. Such variability in the Nd isotopic compositions at site MD95-2002 is in agreement with that encountered in both the modern river and LGM glacigenic sediments (Figs 4 and 5). In detail, ε_{Nd} values decrease during stadial intervals, especially during HS3 (~31-29 ka, ε_{Nd} down to -13.1), HS2 (~26-23 ka, ε_{Nd} down to -12.7) and the early part of HS1 (between 18.2 ± 0.2 and 16.7 ± 0.2 ka, ε_{Nd} down to -14.2). Significant excursions (ε_{Nd} down to -14.1) also occur at the end of the LGM, between 22.5 ± 0.2 to 21.3 ± 0.2 ka and between 20.3 ± 0.2 to 18.7 ± 0.3 ka. We discuss the paleoenvironmental meaning of the evolution of the Nd isotopic compositions at site MD95-2002 below. Note that we specifically focus our interpretation for sediment older than 16.7 ± 0.2 ka (see below). From this time onwards and until the Early Holocene, the sedimentation in the deep Bay of Biscay is strongly affected by the erosion of the shelf deposits (including the lowstand Channel River delta) in response to the significant sea-level rise and the embayment of the English Channel (Bourillet et al., 2003; Toucanne et al., 2012). For this reason, we do not interpret the MD95-2002 ε_{Nd} record throughout the last transgression.

5. DISCUSSION

5.1 Linking Channel River meltwater discharge and EIS fluctuations

5.1.1 EIS fluctuations and the MD95-2002 ε_{Nd} record

The ε_{Nd} detrital value (-11.1) determined for core MD95-2002 surficial sediments (dated at ca. 1.6 ka) is very similar to those measured in sediment layers from the Mid and Early Holocene (about ε_{Nd} -11.6) and from the core-top of a nearby sedimentary record (ε_{Nd} -10.9; KECP-11, see Freslon et al., 2014). Taken together, these data indicate that a ε_{Nd} value of about -11.2 ± 0.4 (1SD) at site MD95-2002 is representative for the present interglacial, and can be used as an estimate for the Nd isotopic signature of river-borne particles delivered to the coring site by rivers from the NW European margin during highstand conditions. This latter assumption is supported by our compilation of the Nd isotopic compositions of modern rivers (Table 2). By considering the Channel River as the main sediment source for the Bay of Biscay during glacial lowstands (Toucanne et al., 2010), we thus assume that sediment deposited at site MD95-2002 during the last glacial and characterised by ('interglacial') ε_{Nd} values around -11.2 ± 0.4 likely indicate a minor contribution of sedimentation from the EIS. Such 'interglacial' ε_{Nd} value characterises the sediment deposited at site MD95-2002 before ca. 32 ka. On the contrary, the MD95-2002 ε_{Nd} record shows significant millennial-scale excursions towards both more negative and positive ε_{Nd} values, ranging from -14.2 to -9.7 from 32 ka onwards (until about 11 ka). The observed ε_{Nd} changes resemble the high-resolution XRF Ti/Ca and Fe/Ca records, suggesting that variations in terrigenous inputs are related to changes in the sediment provenance. Changes in both the ε_{Nd} and the XRF Ti/Ca and Fe/Ca ratios at site MD95-2002 occur concomitantly with changes in the elemental composition (Ti/Ca and Fe/Ca ratios; Figs 4 and 5) in turbidite-rich sequences from the deep Bay of Biscay (i.e., cores MD03-2690 and MD03-2695; Fig. 1) and increases in the turbiditic frequency at these sites (Toucanne et al., 2012; Toucanne et al., 2008; Fig. 4), implying that they represent peak discharges of the Channel River. Overall, these observations suggest that large changes related to ice-marginal fluctuations of the EIS occurred in the Channel River drainage basin at the end of the last glacial and led to corresponding intensification of Channel River runoff and sediment discharge.

5.1.2 SIS contribution

Recent work has shown that once the EIS had invaded the lowlands (with the attendant increase of the Channel River drainage area), the sediment flux to the Bay of Biscay was driven by meltwater runoff during ice-sheet retreat rather than by ice-sheet volume in the drainage area (Toucanne et al., 2010). This explains why maximum Channel River discharge did not coincide with the LGM (i.e., the EIS failing to release substantial meltwater volumes; Boulton and Hagdorn, 2006; Boulton et al., 2001; Hubbard et al., 2009) but instead with the deglaciation. Sediment budget (Toucanne et al., 2010) and high-resolution multiproxy marine records (Eynaud et al., 2012; Eynaud et al., 2007; Ménot et al., 2006; Zaragosi et al., 2001) have also demonstrated that the impact of the SIS (and specifically its meltwater) on the Channel River activity abruptly decreased at ca. 17 ka. This abrupt diminution of the meltwater runoff is clearly depicted at site MD95-2002 through the strong decrease of both the branched and isoprenoid tetraether (BIT) index (Ménot et al., 2006), a proxy for the relative fluvial input of terrestrial organic matter in the marine environment (Hopmans et al., 2004), and the flux of freshwater alga *Pediastrum* (Zaragosi et al., 2001) (Fig. 5). Considering the new chronostratigraphic framework of core MD95-2002, the timing of this event can be refined to 16.7 ± 0.2 ka. The XRF Ti/Ca and Fe/Ca ratios strongly decrease at that time (i.e., to about 0.073 and 0.75, respectively), which indicate significant decrease in the delivery of terrigenous components from the Channel River at the studied site. Those values, taken together with evidence for the abrupt shutdown of SIS meltwater at 16.7 ± 0.2 ka, could help us to determine the precise timing for peak Channel River discharges related to SIS retreat events throughout the studied period. Indeed, the close evolution of the XRF and ε_{Nd} records in core MD95-2002 strongly suggest that variations in terrigenous inputs are related to changes in the sediment provenance. As a result, one can assume that values higher than ca. 0.073 for Ti/Ca and ca. 0.75 for Fe/Ca in core MD95-2002, highlighted as runoff event R1 to R5 in Fig. 4, likely indicate SIS meltwater discharge. The enhanced Channel River runoff during the R1 to R5 events is supported both by the parallel increase of the BIT-index (Ménot et al., 2006) and the flux of freshwater alga *Pediastrum* at site MD95-2002 (Zaragosi et al., 2001) and the increase of the turbidite frequency in the deep Bay of Biscay (Fig. 5). Our determination of the runoff events, based on XRF ratios detailed in Fig. 4, is strongly supported by the isotopic dataset. Maxima in the XRF records (i.e., Ti/Ca > 0.073 and Fe/Ca > 0.75; R1 to R5 events in Fig. 4) correspond to minima in the Nd isotopic compositions [mean ε_{Nd} value of -12.7 ± 0.9 (n = 53), with ε_{Nd} values down to -14.2; Figs 4 and 5]. Only a slight lag (0.5 kyr maximum) between the Nd isotopic compositions and the XRF records is seen for the R4 event (20.3 ± 0.2 to 18.7 ± 0.3 ka), thus questioning the temporal limits of this event. Nevertheless, for this time interval, the uncertainty of these limits (0.5 kyr maximum) is in the range of that (up to 0.4 kyr) of the MD95-2002 chronology (Fig. 3). Moreover, the R1 to R5 events defined by the XRF ratios include > 85 % of the MD95-2002 sediment samples (older than 16.7 ± 0.2 ka; see above) with an ε_{Nd} signature of possible SIS source. The Nd isotopic compositions of potential source regions (Fig. 6; Tables 2 and 3) show that the river-borne particles delivered to the coring site during the R1 to R5 events were derived mainly from east of the Dover Strait, precisely from the North Sea region [-12.2 ± 1.5 (and -13.1 ± 0.8 for East UK) for LGM glacigenic sediments] and the North European Plain [-13.4 ± 1.9 for modern rivers, and from -14.8 ± 1.3 (western part) to -15.1 ± 0.8 (eastern part) for LGM glacigenic sediments].

Both the BIIS (e.g., Clark et al., 2012a) and the SIS (e.g., Sejrup et al., 2000; Sejrup et al., 2009) invaded the North Sea basin during the Pleistocene leading to southwards routing of the

North Sea fluvial systems through the Dover Strait (Busschers et al., 2007; Gibbard, 1988; Gupta et al., 2007; Toucanne et al., 2009a; Toucanne et al., 2009b; Toucanne et al., 2010). As a consequence, the North Sea basin then connects the Channel River to the North European Plain and the extensive southern margin of the SIS (Toucanne et al., 2010). Recent results show that the North Sea was covered by ice during the last glacial period, from ca. 30 to 18-16 ka (Bradwell et al., 2008; Carr et al., 2006; Clark et al., 2012a; Graham et al., 2010). On this basis, we conclude that peak Channel River discharges R1 to R5 identified from 30.7 ± 0.7 to 28.9 ± 0.4 ka (R1), from 24.3 ± 0.3 to 23.4 ± 0.3 ka (R2; see below for details concerning these temporal limits), from 22.5 ± 0.2 to 21.3 ± 0.2 ka (R3), from 20.3 ± 0.2 to 18.7 ± 0.3 ka (R4) and from 18.2 ± 0.2 to 16.7 ± 0.2 ka (R5) are related to SIS retreat events (Figs 4 and 5; Table 4).

Interestingly, minima in the Nd isotopic compositions of the R2 to R5 events gradually increases (i.e., ε_{Nd} down to -12,7, -13.4, -14,1 and -14,2 during the R2, R3, R4 and R5 events, respectively). This could indicate that the SIS contribution in peak Channel River discharges increased through time. By considering the unradiogenic character of the drainage basins of the eastern North European Plain in comparison to those of the western North European Plain (Table 2), this could also highlight (for a strict SIS source) the increasing contribution of the southeastern sector of the ice-sheet. In such a case, a significant contribution of the southeastern sector of the SIS is expected for the R3, R4 and R5 event while a southwestern contribution is likely for R2. These hypothesis are confronted with paleogeographical reconstructions in the following discussion (see discussion, part 5.2).

5.1.3 BIIS contribution

The high ε_{Nd} values (up to -9.6) found between about 28.5 ka and 24 ka indicate the contribution from of a source distinct from both the 'interglacial' riverine background and the

SIS. By considering both the geographical distribution for European ice-sheets during the last glacial (Ehlers et al., 2011) and the Nd isotopic compositions of potential source regions (Figs 5 and 6; Tables 2 and 3), we propose that the river-borne particles delivered to site MD95-2002 during this interval were derived mainly from the western British Isles and the western BIIS (Figs 4 and 5). Recent compilations suggest that western sectors of the BIIS first reached their local last glacial maxima ca. 28-25 kyr ago (Clark et al., 2012a; Clark et al., 2012b; Clark et al., 2009; McCabe et al., 2007; Scourse et al., 2009). Chiverrell et al. (2013), using a Bayesian statistical integration of chronological data, also show a simultaneous southwards advance of the ISIS in Channel River basin. The latter caused deposition of the Irish Sea Till (O'Cofaigh and Evans, 2007; O´Cofaigh and Evans, 2001), which shows ε_{Nd} signature varying from -11.6 to -0.6 along south coast of Ireland (Table 3). This ice-advance was followed by a rapid retreat northwards during HS2 (Scourse et al., 2000), after ca 25.3-24.5 ka, which lead to ice-free conditions in the present-day Celtic Sea no later than ca 23.7-22.9 ka (Chiverrell et al., 2013). Our data supports these reconstructions since the fluctuations of both the MD95-2002 ε_{Nd} record and the turbidite flux in the northern Bay of Biscay probably reflect extensive ice cover over Ireland just before HS2 then meltwater reworking of the Irish Sea Till in the course of the ISIS retreat. Interestingly, the collapse of the ISIS (i.e., ca. 24.5-23.7 ka) modelled by Chiverrell et al. (2013) appears to occur simultaneously with a prominent reversal of the Nd isotopic compositions (ε_{Nd} up to -10) at site MD95-2002. Since this event is stratigraphically embedded within the R2 interval (24.3 ± 0.3 to 23.4 ± 0.3 ka) of SIS origin (ε_{Nd} down to -12.7), we define now the R2 interval as a mixed-source deposit related to a simultaneous retreat of the southern margins of the BIIS and SIS. Thus, the significant gradual decrease in ε_{Nd} from -9.9 to -12.7 between 26.3 ± 0.3 ka and 24.3 ± 0.3 ka likely highlights a mixing of BIIS- and SIS-sourced sediment, with the progressive dominance of the latter. This period was characterized by increased turbidite frequency (Toucanne et al., 2012; Toucanne et al., 2008) and higher flux of freshwater alga *Pediastrum* (Zaragosi et al., 2001) and terrestrial-derived organic matter (i.e., increased BIT-index; Ménot et al., 2006) at site MD95-2002 (Fig. 5). This suggests that the simultaneous ice retreat in Ireland and the North European Plain began earlier than 24.3 ± 0.3 (i.e., lower boundary of the R2 event). As a result, we consider that the abrupt increase of the turbiditic activity dated at 25.7 ± 0.3 ka corresponds to the onset of this regional ice-sheet retreat. Based on these conclusions, we propose that the timing for the R2 event is now defined from 25.7 ± 0.3 ka to 23.4 ± 0.3 ka (Fig. 5 and Table 4).

5.2 Revisiting the pattern and timing of retreat of the EIS, with a specific focus on the SIS

Most NH ice sheets had advanced to near their LGM extents by ca. 26 kyr ago according to Clark et al. (2009). Using an extensive compilation of geochronological constraints, the same authors show that the LGM in the western British Isles and the Baltic lowlands was reached from ca. 28.3-28.1 ka and ca. 27.3-25.3 ka, respectively. We have shown previously, in agreement with the modelled chronological data of Chiverrell et al. (2013), that a significant retreat from this maximum position occurred along the southern margin of the western British Isles during the R2 event, from 25.7 ± 0.3 ka to 23.4 ± 0.3 ka. Paleogeographical reconstructions demonstrate that this sector of the BIIS continuously retreated from this period onward (Chiverrell et al., 2013; Clark et al., 2012a; Clark et al., 2012b). As a result, we assume that the timing of the retreat of the ISIS from 25.7 ± 0.3 ka, that corresponds chronologically with the HS2 (Scourse et al., 2000), provides a new independent constraint for the timing of the early deglaciation of the south-western BIIS.

Contrary to the BIIS (e.g., Clark et al., 2012a), no comprehensive reconstruction for SIS advance and retreat exist to date. As a result, the precise timing for SIS fluctuations during the last termination is still debated (e.g., Böse et al., 2012; Houmark-Nielsen et al., 2006; see Fig. 7 for a thorough review). We have shown previously that the R2 event also probably corresponds to an ice-marginal retreat of the SIS, and of its southwestern sector in particular. The R2 event probably correlates with the ice-margin retreat limited to the North Sea (Sejrup et al., 2009) and the southwest Scandinavia (Ribjerg Fm; Houmark-Nielsen and Kjær, 2003; Larsen et al., 2009) between ca. 27-23 ka. By considering the timing of the onset of the LGM extent in the Baltic lowlands ca. 27.3-25.3 kyr ago (Clark et al., 2009), we assume that this ice-margin retreat, dated here at ca. 25.7 ± 0.3 ka (and until 23.4 ± 0.3 ka), likely provides a chronological constraint for the early deglaciation of the SIS. However the ice retreat observed in southwest Scandinavia between ca. 27-23 ka is known to precede the maximum SIS advance in Denmark (Main Advance, ca. 23-21 ka; Houmark-Nielsen and Kjær, 2003; Larsen et al., 2009) that is coeval with the local last glacial maxima in Germany and Poland (Brandenburg-Leszno Phase, ca. 25-20 ka; Böse et al., 2012) according to Houmark-Nielsen and Kjaer (2003). As a result, the R2 event (and possibly the R1 event as well) is considered to represent a halt (from ca. 25.7 ± 0.3 to 23.4 ± 0.3 ka) in the final advance of the SIS to its LGM position (i.e., the Brandenburg-Leszno ice-marginal position -IMP- in Germany and Poland, which corresponds to the Main Stationary Line in Denmark; Houmark-Nielsen, 2010; Houmark-Nielsen and Kjær, 2003). This ice-marginal retreat is probably limited to the southwestern sector of the SIS according to field observation (Houmark-Nielsen and Kjær, 2003; Larsen et al., 2009; Sejrup et al., 2009) and the ε_{Nd} signature (-12.7) of the corresponding peak in Channel River discharge.

The Nd isotope compositions of the R3 event (ε_{Nd} down to -13.4) likely indicate that the subsequent ice-marginal retreat of the SIS (i.e., from 22.5 ± 0.2 to 21.3 ± 0.2 ka) propagates eastwards. Interestingly, the R3 event coincides within age uncertainties with the retreat from LGM moraines in Belarus and Lithuania dated at 22.1 ± 1.9 ka by Carlson and Winsor (2012) through the new calibration of ^{10}Be ages of Rinterknecht et al. (2006). Taken together with the maximum ice advance over Denmark, Germany and Poland dated after ca. 23.4 ± 0.3 ka (i.e., upper limit of the R2 event), the R3 event allows establishment of the precise timing for the onset of the SIS retreat at the end of the LGM at 22.5 ± 0.2 ka (Figs 4 and 5, and Table 4). This gives an upper-limit age for the LGM moraines in the Baltic lowlands and indicates by extension that the succession of the R3, R4 and R5 events, all interpreted as ice-marginal retreat in the Baltic lowlands, provides an unique opportunity for reconstruction of the decay of the SIS during the course of the last deglaciation. The succession of meltwater events R3 to R5 reveals that the latter was discontinuous in character. This result is strongly supported by the latest glacial morphostratigraphy in the Baltic lowlands that shows a succession of three moraine belts (namely Brandenburg-Leszno, Frankfurt-Poznan, and Pomeranian in Germany and Poland; Figs 1 and 6), successively younger from south (i.e., LGM) to north, indicating that the SIS margin paused twice during its overall deglacial retreat (see Ehlers et al., 2011a for a thorough review).

The initial retreat of the SIS margin at the end of the LGM (i.e., 22.5 ± 0.2 ka) was probably limited in extension. Indeed, the peak Channel River discharge at that time (i.e., R3 event) is relatively weak as suggested by the limited input of sediment and organic material in the Bay of Biscay (Fig. 5). On the contrary, the SIS receded substantially during the subsequent R4 (ca. 20.3 ± 0.2 to 18.7 ± 0.3 ka) and R5 events (ca. 18.2 ± 0.2 to 16.7 ± 0.2 ka), releasing large amounts of meltwater via ice-marginal valleys from the Baltic lowlands to the North Atlantic. At site MD95-2002, these meltwater fluxes are reflected by the shift towards lower ε_{Nd} values (down to -14.2), the deposit of thick laminated facies (Toucanne et al., 2009a; Zaragosi et al., 2001), as well as by the marked increase in the freshwater alga *Pediastrum* (Zaragosi et al., 2001) and in the amount of terrestrially-derived organic matter (i.e., increased BIT-index; Ménot et al., 2006). The few excursions towards more positive ε_{Nd} values during the R5 event indicate that BIIS (or even the Alpine Ice Sheet through the Rhine River; e.g., Busschers et al., 2007) may also have participated in this meltwater pulse.

These events, taken together with the millennial-scale intervals of Channel River shutdown between 21.3 ± 0.2 and 20.3 ± 0.2 ka, and between 18.7 ± 0.3 and 18.2 ± 0.2 ka, probably mirrored the fluctuating retreat and re-advance of the SIS from which the moraine belts originated (Fig. 5 and Table 4). Based on our dataset, we propose that the southern SIS definitely retreated from the Brandenburg-Leszno IMP no later than ca. 20.3 ± 0.2 ka (i.e., R4 event). The end moraines of the Frankfurt-Poznan Phase, usually considered to represent landforms created by an oscillation during the ice retreat from the maximum Brandenburg-Leszno IMP (Ehlers et al., 2011b), could thus correlate with the short pause in the deglaciation observed from ca. 18.7 ± 0.3 ka (i.e., end of the R4 event) to ca. 18.2 ± 0.2 ka (i.e., onset of the R5 event). This event also probably equates with the East-Jylland re-advance in Denmark (Houmark-Nielsen and Kjær, 2003; Larsen et al., 2009) (Fig. 7). The subsequent SIS retreat occurring from ca. 18.2 ± 0.2 to 16.7 ± 0.2 ka (i.e., the R5 event) probably led to ice-free conditions north of the Polish Baltic coast prior to the subsequent Pomeranian ice-advance (Rinterknecht et al., 2006). The pulse of meltwater probably lasted until the disappearance of the ice tongue established over the modern North Sea region. Since then, it is likely that SIS meltwater was diverted towards the Nordic Seas. This coincides with the observed cessation of Channel River activity (Toucanne et al., 2010). Nevertheless, recent reconstruction of the SIS in the East European Plain reveals that the receding margin paused between 17.2 ± 0.4 and 15.7 ± 0.3 ka, during the Pomeranian phase (Soulet et al., 2013), in good agreement with new exposure ages for this moraine (16.4 ± 1.2 ka to 15.6 ± 0.6 ka) (Rinterknecht et al., 2013; Rinterknecht et al., 2012), allowing for the possibility of the Channel River cessation due to another pause in the retreat of the SIS.

The correlations between our MD95-2002 record and the moraine belts should be taken with caution with regard to the complexity of the morphostratigraphy in the Baltic lowlands (e.g., see Ehlers et al., 2011b for a thorough review in Northern Germany). Nevertheless, our chronology for retreat and re-advance of the SIS throughout the deglaciation reconciles most of the earlier chronological reconstructions proposed all along the southern SIS margin (see Fig. 7 and the associated references). Thus, the millennial-scale timing for discrete input of sediment-laden meltwater of SIS origin in the Bay of Biscay reveals that the whole southern SIS margin fluctuated synchronously (during the R3, R4 and R5 events in particular), likely in response to changes in the mass balance of the Baltic Sea Ice Stream (Boulton et al., 2001). Interestingly, core MD01-2461 located off Ireland shows peaks of BIIS-sourced IRD commencing at ~22.4 ka, ~20.3 ka and ~18.4 ka, which lasted between 1.6 to 1.0 kyr (Peck et al., 2006) and correlated with the R3, R4 and R5 events, respectively. This reveals synchronous instability of both the eastern (i.e., SIS) and western (i.e., BIIS) parts of the EIS, thus pointing out that the EIS as a whole was responding to a large-scale climate forcing. This result as well as its consistency with regard to the chronology of the LIS (discussed below) strongly challenges the emerging view for time-transgressive ice-sheet fluctuations in Europe during the deglaciation (Böse et al., 2012). The mixing of various types of material (boulders, quartz, feldspars, wood, plant detritus, bones, shells, etc.) and various methods (^{10}Be, ^{36}Cl, ^{26}Al, OSL, IRSL, ^{14}C) - with their own uncertainties regarding both the age (depending of e.g. cosmogenic radionuclide production rate) and their interpretation (e.g., Heyman et al., 2011; Houmark-Nielsen et al., 2012) - to date the continental glacigenic deposits originated from the rapid ice-marginal fluctuations of the SIS discussed above likely explains most of the chronological discrepancies recently highlighted along the SIS moraine belts (Böse et al., 2012). A summary for the timing of SIS fluctuations recognised on land [i.e., Pomeranian, Frankfurt-Poznan, Brandenburg-Leszno (e.g., Ehlers et al., 2011b; Houmark-Nielsen and

Kjær, 2003) and even Kattegat and Klintholm phases (Houmark-Nielsen, 2010; Möller and Murray, 2015)] is proposed in Figs 5 and 7, and Table 4.

5.3 Comparing the timing of retreat of the SIS and LIS

The pattern of ice-margin retreat for the southern SIS margin, with initial retreat at 22.5 ± 0.2 ka followed by more extensive retreat after 20.3 ± 0.2 ka, is similar in timing to that of the southern LIS margin (Carlson and Winsor, 2012; Curry and Petras, 2011; Ullman et al., 2015). Recent compilation of ^{10}Be surface exposure ages focusing on southern LIS lobes reveal that the southern LIS began retreating at 23.0 ± 0.6 ka (Ullman et al., 2015). This initial retreat, concomitant with the R3 event in Europe, was limited during the next ~3 kyr, but was then followed by more rapid retreat (e.g., by 19.4 ± 0.7 ka for the southern Green Bay Lobe). The detailed comparison of our SIS retreat chronology with those of the well-dated Lake Michigan and Miami-Scloto lobes (Ullman et al., 2015) show that large-scale recessions of the southern LIS coincide within age uncertainties with the R4 and R5 events in Europe (Fig. 5). The latter event also coincides with a rapid deglaciation (50-100 m/yr) of central Connecticut, southeastern LIS (Ridge et al., 2012). In addition, massive discharges of freshwater in the northeast Pacific also reveal enhanced ablation of the Cordilleran Ice-Sheet during these two intervals (Lopes and Mix, 2009). Thus, both the timing for the early deglaciation (from 23.0 ± 0.6 ka and from 22.5 ± 0.2 ka in North America and in Europe, respectively) and the acceleration of the margin retreat on both sides of the North Atlantic (from 20.4 ± 0.3 ka and from 20.3 ± 0.2 ka in North America and in Europe, respectively) occurred simultaneously. Recent climate-surface mass balance simulations revealed that the small increase in northern summer insolation ca. 24-23 ka (Fig. 5), and the acceleration in rising insolation thereafter (i.e., ca. 20 ka), is potentially sufficient to explain the deglacial pattern of the LIS (Abe-Ouchi et al., 2013; Ullman et al., 2015). The similar timing observed for retreat of the LIS and SIS, by excluding local climate anomaly or dynamic instability as possible forcings, strongly supports this assumption. In addition, the similar timing for enhanced margin retreat on both sides on the North Atlantic supports the contention that the EIS, together with the LIS, was an important source for the 5-10 m eustatic sea-level rise that occurred sometime between 20 and 19 ka (Carlson and Clark, 2012; Clark et al., 2004b; Yokoyama et al., 2000).

Finally, our dataset reveals that some significant ice-sheet fluctuations occur simultaneously on both sides of the North Atlantic before the deglaciation, precisely during HS3 and HS2 that correspond to our R1 (ca. 30.7 ± 0.7 to 28.9 ± 0.4 ka) and R2 (ca. 25.7 ± 0.3 to 23.4 ± 0.3 ka) events, respectively. The latter coincides with discharge of icebergs from the Hudson Strait Ice Stream of the LIS to the North Atlantic (i.e., HE's; Andrews and Tedesco, 1992; Hemming, 2004). These events occurred at the same time that northern summer insolation declined (Fig. 5), thus pointing out a different forcing for these ice-marginal fluctuations. For HS2, Scourse et al. (2000) identifies glacio-eustatic sea-level rise associated with the LIS discharge icebergs through Hudson Strait as a possible feedback mechanism causing destabilisation of marine-terminating ice-streams including the ISIS. However, the ε_{Nd} signature of the Channel River meltwater discharges during HS3 and HS2 suggests a significant retreat of the Baltic Ice Stream in the North European lowlands, thus showing that not only marine-terminating ice-streams are involved in these events. Ice lobes from the southwestern LIS (e.g., Puget Lobe of Cordilleran Ice Sheet) began to retreat at about the time of HS (Clark and Bartlein, 1995), producing massive discharges of freshwater in the northeast Pacific (Lopes and Mix, 2009). This supports the synchroneity of ice-sheet fluctuations on both sides of the North Atlantic, and the participation of terrestrial-terminating ice-streams during HS3 and HS2. We discuss the implications of this result below.

5.4 Role of the EIS during the last deglaciation

We have demonstrated previously that each substantial injection of meltwater to the North Atlantic via the Channel River since the LGM was linked directly to ice recession of the southern EIS margins. Our ε_{Nd} proxy record for core MD95-2002 allows one to compare the evolution of the EIS with well-dated paleoclimatic and paleoceanographic records and hence to explore its role in the first steps of the last termination.

The last two EIS retreat (i.e., R4 and R5) events that led to increased meltwater discharges to the North Atlantic occurred at the same time as sharp decreases in sea-surface salinity (Fig. 8e) (Eynaud et al., 2012) and, within age model uncertainties, southward shifts of the polar front in the eastern North Atlantic (Fig. 8c,d) (Bard et al., 2000; Eynaud et al., 2009). Both events correspond to periods of proposed AMOC weakening (Fig. 8f) (Hall et al., 2006; McManus et al., 2004), suggesting that the EIS, in addition to the LIS (Carlson and Winsor, 2012; Clark et al., 2007), could have affected the AMOC at the very beginning of the last termination (Roche et al., 2010) with farfield effects as suggested by the concomitant weakening / strengthening of the Chinese / Australasian monsoon, respectively (Fig. 8h) (Ayliffe et al., 2013; Wang et al., 2001). The last major episode of meltwater discharge that freshened sea-surface waters occurred between 18.2 ± 0.2 and 16.7 ± 0.2 ka, thus coinciding with the first part of HS1. The persistent EIS melting during the first part of HS1 (as well as during HS2 and HS3), well known as having been a very cold and arid event in the North Atlantic region (Bard et al., 2000), likely involved the role of seasonality (Denton et al., 2005) in a winter-centric mode. Concerning HS1, increasing boreal insolation would have sustained summer warming and attendant ice-margin melting. In turn, early meltwater released to the North Atlantic by decreasing the AMOC rate and northward oceanic heat transfer would have caused hyper-cold winters (Denton et al., 2010). The latter is suggested by the concomitant expansion of sea-ice cover in the northern Atlantic region including the Bay of Biscay (Fig. 8b) (Zaragosi et al., 2001). The deposition of a thick, laminated sediment layer at site MD95-2002 between 18.2 ± 0.2 and 16.7 ± 0.2 ka, interpreted as the result of seasonal spring-summer meltwater discharges from the Channel River (Toucanne et al., 2009a; Zaragosi et al., 2001), as well as the retreat of the eastern edge of the EIS at the same time (Soulet et al., 2013) supports the winter-dominated seasonality mechanism as a cause for ice sheet deglaciation in 'apparent' cold climate conditions. Such a mechanism also probably explains the rapid retreat of the North American ice sheets observed after 18.4 ± 0.8 ka (Lopes and Mix, 2009; Ridge et al., 2012; Ullman et al., 2015). Of particular interest, the early HS1 major meltwater event predated LIS iceberg outbursts (HE1) by some 1,500 years (Fig. 8b). In core MD95-2002, this fact is robustly supported because the results of such outbursts are observable in the core stratigraphy. Indeed, the laminated sediment layer recording seasonal Channel River floods during the period of highest activity (i.e., R5 event) is overlain by LIS IRD (after 16.7 ± 0.2 ka) (Grousset et al., 2000; Zaragosi et al., 2001). Also, the regional sea-surface salinity signal in Fig. 8e, derived from the same core, shows that the observed freshening started well before IRD deposition. The recorded major meltwater pulse is coeval both with the AMOC weakening as suggested by both Pa/Th measurements on either side of the Atlantic (Hall et al., 2006; McManus et al., 2004) and flow strength reconstruction (Fig. 8f) (Praetorius et al., 2008), and with surface and intermediate water warming in the western (sub-) tropical Atlantic (Fig. 8g) (Carlson et al., 2008; Marcott et al., 2011; Rühlemann et al., 1999). Based on these considerations, we propose the following scenario. About 18 ka, the Channel River system underwent deglacial reactivation in response to the rapid, large-scale recession of the SIS. This, added to the simultaneous rapid melting of the southern LIS (Carlson and Winsor, 2012; Clark et al., 2007; Ullman et al., 2015) and the instability of BIIS ice-streams (Hall et al., 2006; Peck et al., 2006; Scourse et al., 2009), led to a period of

~1,500 years of near-continuous meltwater injection into the North Atlantic, resulting in surface water freshening that could have weakened the AMOC and thereby reduced northward oceanic heat transport. As a consequence, the (sub-) tropical Atlantic Ocean probably warmed and, even if reduced, the northern export of warm tropical waters along the NE coast of North America was sufficient to trigger the destabilisation of the LIS marine-based ice streams (Clark et al., 2007) as suggested by recent modelling studies (Alvarez-Solas et al., 2010; Alvarez-Solas et al., 2013; Marcott et al., 2011). Hence, after 16.7 ± 0.2 ka (i.e., end of the R5 event), the massive LIS iceberg surge (HE1; centred at 16-15.5 ka according to Carlson and Clark, 2012) injected large volumes of meltwater into the North Atlantic that sustained AMOC reduction (McManus et al., 2004) and NH stadial conditions until ca. 15 ka. The impact of the Channel River meltwater discharges in the initial event of this scenario is potentially possible given that AMOC is sensitive to freshwater perturbations along the western European margin (Roche et al., 2010) and that the Channel River water discharge at that time (up to 0.4 Sv; Toucanne et al., 2010) was presumably higher than the necessary threshold to affect AMOC [~0.15 Sv in the Bay of Biscay, see Roche et al. (2010); from 0.05 to 0.3 Sv more generally, see Ganopolski and Rahmstorf (2001), Levine and Bigg (2008), Rahmstorf (1995) among others]. Our findings support results showing that iceberg discharges, or so-called HE's, were the consequence of stadial conditions rather than the cause (Alvarez-Solas et al., 2013; Barker et al., 2015; Bond and Lotti, 1995; Clark et al., 2007).

The meltwater-induced weakening of the AMOC leading to the winter-centric HS1 in the North Atlantic region is correlative with a significant bipolar seesaw response (Shakun et al., 2012) as shown with the concomitant widespread oceanic/atmospheric warming in the SH (Fig. 8h,i) (Ayliffe et al., 2013; Barker et al., 2009) and large-scale recession of glaciers in Patagonia and New-Zealand (Hall et al., 2013; Putnam et al., 2013). Similarly the first significant NH ice-sheets retreats recorded at ~22 ka and ~20-19 ka likely triggered a bipolar seesaw response in the SH. Indeed, Channel River meltwater discharges during these intervals (i.e., R3 and R4 events) appear to be nearly synchronous with the first deglacial seesaw events marked in the SH by southward shifts of oceanic/atmospheric fronts (Fig. 8h,i) (Ayliffe et al., 2013; Barker et al., 2009; Shakun et al., 2012), glacier recession in Patagonia (Denton et al., 1999; Murray et al., 2012), and warming of Antarctica (Fig. 8j) (WAIS-Divide-Project-members, 2013; Weber et al., 2014). At the same time, weakening of the summer monsoon is observed in the NH, especially in East Asia (Duan et al., 2015; Wang et al., 2001). Taken together with the slight AMOC perturbations observed during these intervals (Fig. 8f) (Hall et al., 2006; McManus et al., 2004; Praetorius et al., 2008), our dataset emphasises the high sensitivity of global climate to meltwater releases in the North Atlantic. Similarly, as discussed for HS1 and the delayed discharge of icebergs from the LIS, the retreat of the EIS southern margin and corresponding Channel River meltwater discharges during HS3 and HS2 could have caused the reduction in AMOC responsible for the marine-based ice stream purge cycle (i.e., HE's; Alvarez-Solas et al., 2010; Alvarez-Solas et al., 2013; Barker et al., 2015; Marcott et al., 2011). All the above suggests that the EIS together with the LIS drove climate changes at the end of the last glacial period, and finally participated in creating the necessary environmental changes in both hemispheres that finally pushed the Earth out of the last ice age.

6. CONCLUSION

Our Nd isotope record of Channel River meltwater discharges to the North Atlantic provides, after comparison with continental morphostratigraphical evidences and associated glacigenic samples, a continuous and well-dated record for the evolution of the EIS southern margin through the end of the last glacial period and during the deglaciation. Importantly, our results show that the pattern of ice-margin retreat for the SIS is similar in timing to that of the southern LIS margin, with moderate ice-sheet retreat (from 22.5 ± 0.2 ka in the Baltic lowlands) as soon as the northern summer insolation increase (about 23 ka) and an acceleration of the margin retreat thereafter (from about 20 ka). By synchronising ice-marginal fluctuations on land with records of AMOC and climate changes, our data suggest that EIS, together with the LIS, have played a significant role in the first steps of the last termination. EIS recession events in the Baltic lowlands led to substantial injections of meltwater to the North Atlantic via the Channel River between 22.5 ± 0.2 and 21.3 ± 0.2 ka, between 20.3 ± 0.2 and 18.7 ± 0.3 ka, and between 18.2 ± 0.2 and 16.7 ± 0.2 ka with possible subsequent AMOC destabilisation and interhemispheric climate changes. The last EIS meltwater event starting at ca. 18.2 ± 0.2 ka was potentially important enough to trigger a pronounced (in amplitude and duration) interhemispheric seesaw event and the so-called HS1 in the NH, and persisted for a sufficient duration (~1500 years) to allow the subsequent discharge of icebergs from the LIS (HE1) through mid-depth warming in the North Atlantic, thus prolonging HS1 until ca. 15 ka. In addition to providing a possible mechanistic explanation for the exceptional duration of HS1, our results provide support for the view that meltwater-induced weakening of the AMOC were inherent to terminations. Finally, our dataset reveals that significant retreat of the EIS southern margin and concomitant increase Channel River meltwater discharges also occurred during HS3 and HS2. We assume, as discussed for HS1 and the delayed LIS iceberg discharge, that such meltwater events, by involving continental parts of NH ice-sheets, could have functioned as a possible driver of the oceanic perturbations (i.e., AMOC shutdown) responsible for the marine-based ice stream purge cycle, or so-called HE's, that punctuate past glacial periods.

ACKNOWLEDGMENTS

This work was sponsored by the French National Research Agency (ANR) via the ECO-MIST project (#2010-JCJC-609-01). The authors warmly acknowledge those who kindly supplied the continental sediment samples (P. Antoine, F. Buscheers, S. Carr, S. Clerc, C. Dubrulle-Bruneau, J. Ehlers, A. Elverhoi, D.J.A. Evans, M. Frueggard, P.L. Gibbard, A. Groengroeft, H. Hünecke, G. Kowaleska, D. Krzyszkowski, N.K. Larsen, T. Leipe, C. Lüghtens, J.P. Lunkka, C. Mellett, F. Nordblad, C. O'Cofaigh, J. Patzold, D. Richards, M. Rogerson, I. Smith, A. Trentesaux, G. Vaikutiene, H. Vallius, B. Van Vliet-Lanoë, C. Winter, A. Wheeler, W. Wysota and V. Zelchs), E. Ponzevera for assistance on the Neptune MC-ICPMS, C. Skonieczny for XRF acquisition, S. Bermell for mapping, S. Barker, G.H. Denton, P.L. Gibbard, V. Rinterknecht and P.U. Clark for discussions, and the reviewers (C. D. Clark and S. Hemming) for their helpful comments, which greatly improved the manuscript. G.S. acknowledges the Postdoctoral Scholar Program at the Woods Hole Oceanographic Institution, with funding provided by the National Ocean Sciences Accelerator Mass Spectrometry Facility. F.E. acknowledges the European Union's Seventh Framework programme "Past4Future".

FIGURE CAPTION

FIGURE 1. **a**, Palaeogeography of western Europe showing the glacial limits of the European Ice Sheet (EIS) including the Scandinavian (SIS) and British-Irish Ice Sheets (BIIS), the Irish Sea Ice Stream (ISIS) (Boulton et al., 2001; Clark et al., 2012a; Ehlers et al., 2011a), and the Channel River hydrographic network (with ice-marginal valleys -urstromtal- in the North European Plain) during the Last Glacial Maximum (LGM) (Bourillet et al., 2003; Gibbard, 1988; Toucanne et al., 2010). Filled circles and open squares indicate the location of the modern rivers (Table 2) and LGM glacigenic samples (Table 3), respectively (green: western British Isles and ISIS; blue: Baltic lowlands and southern SIS margin; white: downstream part of Channel River, North Sea and inner SIS), used to constrain the provenance of terrigenous input in core MD95-2002 (yellow star). Br.: Brandenburg-Leszno moraine (deposited between 23.4 ± 0.3 and 20.3 ± 0.2 ka), Fr.: Frankfurt-Poznan moraine (from 18.7 ± 0.3 to 18.2 ± 0.2 ka), Pm.: Pomeranian moraine (from 16.7 ± 0.2 to 15.7 ± 0.3 ka), see the main text and Table 4 for details about this chronology. The white crosses in the Bay of Biscay correspond (from west to east) to the location of cores MD03-2692 (Trevelyan Escarpment), MD03-2690 and MD03-2695 (Armorican turbidite system) (Figs 2 and 4, and Table 1). **b**, Location of the main marine sediment records discussed in the text and Fig. 8 (red diamonds). Also shown are the extent of the EIS and LIS (white shading) and a simplified pattern of Atlantic Ocean circulation, with the warm saline waters of the North Atlantic current (red arrows) and the return flow pathway of the deep waters (blue arrows). White arrows indicate the main supply sources of freshwater to the North Atlantic. White crosses indicate the location of cores MD03-2690 and MD03-2692 (Figs 2 and 4; Table 1).

FIGURE 2. Stratigraphic correlation of cores MD03-2692 (left panel) and MD03-2690 (right panel) with core MD95-2002 (Fig. 1), based on the abundance of the planktic polar foraminifera *Neogloboquadrina pachyderma* (left coiling; Nps (%), grey line; Eynaud et al., 2012; Eynaud et al., 2007; Grousset et al., 2000; Mojtahid et al., 2005; Zaragosi et al., 2006; Zaragosi et al., 2001) and the XRF-Ti/Ca ratio (black line; three-points moving average shown as red line; Mojtahid et al., 2005; Zaragosi et al., 2006). Vertical dashed lines represent core-to-core correlations. $^{\mathbf{14}}$C dated samples (Eynaud et al., 2012; Mojtahid et al., 2005; Toucanne et al., 2008; Zaragosi et al., 2006; Zaragosi et al., 2001) are marked by solid circles on the depth scale, with red and blue circles corresponding to ^{14}C dates transferred to core MD95-2002 from core MD03-2692 and core MD03-2690, respectively. YD: Younger Dryas; BA: Bølling-Allerød; HS: Heinrich Stadial.

FIGURE 3. Calendar chronology (black line) and associated error range (2σ; grey shaded area) for core MD95-2002 based on (*i*) correlation with the NGRIP ice core isotopes from Greenland (green probability densities, GICC05 chronology; Andersen et al., 2006; Rasmussen et al., 2006), and (*ii*) calibration of the planktic radiocarbon dates from core MD95-2002 and additional ^{14}C ages from the nearby cores MD03-2690 (Armorican turbidite system) and MD03-2692 (Trevelyan Escarpment) (blue probability distributions; see Figs 1 and 2 for locations and ^{14}C projections, respectively). Information on each age is detailed in Table 1. MD95-2002 chronology was built using the "classical" (non-bayesian) age modeling software Clam (Blaauw, 2010; version 2.2). All radiocarbon age were calibrated after reservoir correction (see the main text for details). ^{14}C age SacA-003247 was removed from final age model because it was clearly an outlier (Table 1). The age-depth model is a smooth spline with the common smoothing parameter 0.3 (Blaauw, 2010) generated through 40.000 iterations. Any model with age-depth reversals was removed. Calculations were performed at

95% confidence. The goodness-of-fit is 23.7 (see Blaauw, 2010 for more information on this parameter). Sediment accumulation rates (SAR; $cm.kyr^{-1}$) for core MD95-2002 are shown. Note that changes in SAR in core MD95-2002 match the evolution of turbidite frequency in the Armorican turbidite system (Figs 4 and 5) (Toucanne et al., 2012; Toucanne et al., 2008). HS: Heinrich Stadial.

FIGURE 4.**A**, **a**, XRF Ti/Ca (red) and Fe/Ca (blue) ratios for turbidite-rich cores MD03-2690 (until ca. 26 ka; continuous lines) and MD03-2695 (only shown for the ca. 22-33 ka interval; dotted lines), Armorican turbidite system (see Fig. 1 for location). Chronology based on correlation with core MD95-2002 (Fig. 2) and supported by ^{14}C ages (see Toucanne et al., 2008 for details). **b**, Turbidite flux off the Channel River (Toucanne et al., 2012; Toucanne et al., 2010). **c**, Neodymium isotopic composition in core MD95-2002 (expressed in ε_{Nd}) as a proxy for Channel River sediment provenance. Mean ε_{Nd} signatures for LGM glacigenic (squares; Table 3) and modern rivers samples (circles; Table 2) from the western British Isles (BIIS; green) and the North European Plain (SIS; blue) are shown on the right. Considering that ε_{Nd} of about -11.2 ± 0.4 provides a mean signature for river-borne particles delivered to the coring site by rivers from the NW European margin during the Holocene, only sediment with ε_{Nd} values higher than about -11 are interpreted from BIIS origin. In contrast, sediment with ε_{Nd} values lower than about -12 are interpreted from SIS origin. **d**, XRF Ti/Ca (red) and Fe/Ca (blue) ratios for core MD95-2002. The dashed lines highlight the boundaries (i.e., Ti/Ca > 0.073 and Fe/Ca > 0.75) used to constraint the Channel River runoff events (R) 1 to 5, interpreted as retreat of the southern EIS (see the main text for details). The latter are highlighted by the vertical blue (SIS-origin) / green (BIIS-origin) bars. The arrows at ca. 16 and 24 ka point out the impact of authigenic precipitation of calcite at site MD95-2002 (Auffret et al., 1996; Toucanne, 2008), that probably correspond to the 'cemented marls' of

Hemming et al. (2004) interpreted as 'Hudson Strait' Heinrich events. **e**, ^{14}C ages with uncertainties, core MD95-2002 (Fig. 3 and Table 1). Note that, for clarity, the age scale between 15 and 23 ka is different from that between 8 and 15 ka and between 23 and 38 ka. **B**, Probability density of the dated levels of the 'deglacial' Channel River runoff event (R) 3 to 5 (see Fig. 3 for the detailed chronology). Vertical scales are arbitrary. YD: Younger Dryas; BA: Bølling-Allerød; HS: Heinrich Stadial; HE: Heinrich Event.

FIGURE 5. **a**, Summer energy (red line, τ=400) (Huybers, 2006) and 21 June-20 July insolation for 55°N (blue line) (Laskar et al., 2004). **b**, Greenland temperature (NGRIP ice core) (NGRIP-members, 2004). **c**, *N. pachyderma* (left coiling) abundance in core MD95-2002 (Zaragosi et al., 2001) tuned to NGRIP ice core record (tuning points -shaded lines-shown) and ^{14}C dates (see in the lower part of the figure; Table 1). **d**, Neodymium isotopic composition in core MD95-2002 (expressed in ε_{Nd}) as a proxy for Channel River sediment provenance. Mean ε_{Nd} signatures for LGM glacigenic (squares; Table 3) and modern rivers samples (circles; Table 2) from the western British Isles (BIIS; green) and the North European Plain (SIS; blue) are shown on the right. Sediment with ε_{Nd} values higher / lower than about -11 / -12 are interpreted from BIIS / SIS origin, respectively. **e**, XRF Ti/Ca (red) and Fe/Ca (blue) ratios for core MD95-2002. The arrows indicate the impact of authigenic precipitation of calcite ('cemented marls' of Hemming, 2004, or 'Hudson Strait' Heinrich events) at site MD95-2002. **f**, Turbidite flux off the Channel River (Toucanne et al., 2012; Toucanne et al., 2010). **g**, Concentration of *Pediastrum* (green line) (Zaragosi et al., 2001) and branched and isoprenoid tetraether (BIT) index (red line) (Ménot et al., 2006) in MD95-2002. **h**, EIS (this study; longitude ~10-20°E) and LIS (Lake Michigan Lobe, LML; Miami-Scloto Lobe, MSL; see Ullman et al., 2015) retreat chronologies; distance north of LGM moraines. Colored circles indicates the timing for the onset of ice-sheet retreat at the end of the LGM. Br.:

Brandenburg-Leszno ice-marginal position -IMP-; Fr.: Frankfurt-Poznan IMP; Pm.: Pomerian IMP. Pre-LGM ice advances of the SIS are also indicated (i.e., Klintholm -Klh.- and Kattegat -Ktt.- ice advances, Denmark; Houmark-Nielsen, 2003; Houmark-Nielsen, 2010; Möller and Murray, 2015). The vertical blue (SIS-origin) / green (BIIS-origin) bars represent the Channel River discharges (i.e., runoff -R- events 1 to 5), interpreted as retreat of the southern EIS. **i**, ^{14}C ages with uncertainties, core MD95-2002 (Fig. 3 and Table 1).

FIGURE 6. **a**, Palaeogeography of western Europe showing the glacial limits of the European Ice Sheet (EIS), including the Scandinavian (SIS) and British-Irish Ice Sheets (BIIS), the Irish Sea Ice Stream (ISIS) (Boulton et al., 2001; Clark et al., 2012a; Ehlers et al., 2011a), and the Channel River hydrographic network (with ice-marginal valleys in the North European Plain) during the LGM (Bourillet et al., 2003; Gibbard, 1988; Toucanne et al., 2010). Filled circles and open squares indicate the location of the modern river (Table 2) and LGM glacigenic samples (till plains, moraines, ice-marginal valleys, outwash plains and proglacial lakes deposited/formed along the southern margin of the EIS; Table 3), respectively (green: western British Isles and ISIS; purple: eastern British Isles and BIIS; orange: English Channel and downstream part of Channel River; grey: south-central North Sea and confluence of the BIIS and SIS; blue: Baltic lowlands and southern SIS margin; red: Scandinavia and inner SIS) used to constrain the provenance of terrigenous input in core MD95-2002 (yellow star). Br.: Brandenburg-Leszno moraine (deposited between 23.4 ± 0.3 and 20.3 ± 0.2 ka), Fr.: Frankfurt-Poznan moraine (from 18.7 ± 0.3 to 18.2 ± 0.2 ka), Pm.: Pomeranian moraine (from 16.7 ± 0.2 to 15.7 ± 0.3 ka; see the main text for details). **b**, Neodymium isotopic composition (expressed in ε_{Nd}) for modern rivers (filled circles; Table 2) and LGM glacigenic samples (open squares; Table 3) according to their location [i.e., longitude; see Fig. 6a]. Mean ε_{Nd} signatures according to the geographic clusters defined in Tables 2 and 3.

FIGURE 7. Summary of regional ice-sheet chronologies for the southern SIS margin between 38 and 14 ka (Middle and Late Weichselian). Chronologies, mixing various types of material (boulders, quartz, feldspars, wood, plant detritus, bones, shells, foraminifera, etc.) and various methods were used (^{10}Be, ^{36}Cl, ^{26}Al, OSL, IRSL, ^{14}C) [Ref. 1: Houmark-Nielsen et al. (2010); 2: Houmark-Nielsen and Kjaer (2003); 3: Marks (2012); 4: Houmark-Nielsen (2003); 5: Larsen et al. (2009); 6: Bradwell et al. (2008); 7: Sejrup et al. (1994); 8: Sejrup et al. (2009); 9: Clark et al. (2012a); 10: Houmark-Nielsen et al. (2012); 11: Lüghtens and Böse (2011); 12: Heine et al. (2009); 13: Litt et al. (2007); 14: Clark et al. (2009); 15: Marks (2002); 16: Wysota et al. (2009); 17: Rinterknecht et al. (2007); 18: Rinterknecht et al. (2006); 19: Carlson and Winsor (2012); 20: Kjaer et al. (2003); 21: Rinterknecht et al. (2012); 22: Nygard et al. (2004); 23: Lüghtens et al. (2011); 24: Rinterknecht et al. (2013); 25: Rinterknecht et al. (2005)]. The LGM sequence is defined by considering the timing of when sectors of the southern SIS (from the North Sea region to the Baltic States) first reached their local last glacial maximum. Pre-LGM and post-LGM sequences are based on sedimentological evidence bracketing the LGM ice advance and retreat sequences. Vertical shaded blue boxes delimit periods (with uncertainties in dark blue) of SIS-derived meltwater input at site MD95-2002, interpreted as ice-sheet retreat in the Baltic lowlands (runoff -R- events 1 to 5). Based on this interpretation, the chronology for core MD95-2002 was used to revisit the timing for ice margin fluctuations in the Baltic lowlands (Table 4). The latter is summarized in the lower part of the figure (blue symbols) with retreat from the Brandenburg-Leszno Moraine in Germany and Poland (i.e., LGM Sequence) from 20.3 ± 0.2 ka, ice advance to the Frankfurt-Poznan ice-marginal position (i.e., Post-LGM Sequence 1) from 18.7 ± 0.3 ka, retreat from the Frankfurt-Poznan Moraine from 18.2 ± 0.2 ka, ice-advance to the Pomeranian Moraine (i.e., Post-LGM Sequence 2) from 16.7 ± 0.2 ka (this study) and subsequent retreat after 15.7 ± 0.3 ka (Soulet et al., 2013). The millennial Nd isotope excursion coupled to high turbidite

flux during HS3 (~31-29 ka) and HS2 (~26-23 ka; Figs 3, 4 and 5) affords robust chronological constraints for pre-LGM ice-marginal fluctuations in Europe [e.g., Klintholm and Kattegat ice advances in Denmark (Houmark-Nielsen, 2003; Houmark-Nielsen, 2010; Möller and Murray, 2015); late Middle Vistulian in Poland (Marks, 2012); Rogne Stadial in western Norway (Mangerud et al., 2010)]. Note that the younger episode (i.e., HS3) is synchronous with the boundary between the Middle and the Upper Würmian in the Alps (Spötl et al., 2013), as well as with the timing of the Middle-Upper Pleniglacial transition in central Europe (Kadereit et al., 2013).

FIGURE 8. **a,** Greenland oxygen isotopes (NGRIP ice core; NGRIP-members, 2004). **b,** Ice-rafted debris (black line; Zaragosi et al., 2001), BIT-index (red line; Ménot et al., 2006) and concentration of the polar dinocyst specie *Islandinium minutum* (green line; Auffret et al., 2002; Eynaud, 1999; Zaragosi et al., 2001), a proxy for sea-ice cover (>6 months/yr; Rochon et al., 1999), in MD95-2002. **c,** NE Atlantic sea surface temperature (core SU8118, Fig. 1; Bard et al., 2000). **d,** *N. pachyderma* (left coiling) abundance (core MD95-2002; Zaragosi et al., 2001). **e,** Sea surface salinity (core MD95-2002; Eynaud et al., 2012). **f,** Proxies for AMOC strength : ^{231}Pa/^{230}Th ratio at site OCE326-GGC5 (blue line, Fig. 1; McManus et al., 2004) and DAPC2 (grey line, Fig. 1; Hall et al., 2006), and grain-size data (i.e., flow strength, purple line) from ODP Site 984, Southern Iceland (Praetorius et al., 2008). **g,** Western tropical Atlantic SST (core M35003-4, Fig. 1; Rühlemann et al., 1999). **h,** Stalagmite oxygen isotopes from Flores, Indonesia (Ayliffe et al., 2013). **i,** SE Atlantic polar foraminifera species (core TNO57-21, Fig. 1; Barker and Diz, 2014; Barker et al., 2009). **j,** West Antarctica oxygen isotopes (WAIS Divide ice core) (WAIS-Divide-Project-members, 2013). The vertical blue bars represent the Channel River discharges (i.e., runoff -R- events 3 to 5), interpreted as retreat of the southern SIS.

TABLE CAPTION

TABLE 1. Calibration of ^{14}C dates [Ref. 1: Zaragosi et al. (2001); 3: Zaragosi et al. (2006); 4: Toucanne et al. (2008); 5: Eynaud et al. (2007); 6: Grousset et al. (2000); 8: Auffret et al. (2002)] was performed using Clam software (Blaauw, 2010) with the IntCal13 calibration curve (Reimer et al., 2013) (see part 3 for details). NGRIP tie-points (i.e., onset of Greenland Interstadials, GI) and associated uncertainties (2σ) according to Rasmussen et al. (2006 ; Ref. 2 in the table) and Andersen et al. (2006 ; Ref. 7).

TABLE 2. Neodymium isotope signature of the clay-silt fraction (<63µm) of some European rivers. Measured $^{143}Nd/^{144}Nd$ ratios are reported in ε_{Nd} notation, $[(^{143}Nd/^{144}Nd)_{sample}/(^{143}Nd/^{144}Nd)_{CHUR} - 1] \times 10^4$, using $(^{143}Nd/^{144}Nd)_{CHUR} = 0.512638$ (Jacobsen and Wasserburg, 1980). Geographic clusters (with weighted mean ε_{Nd} signature considering the river drainage surface) correspond to potential sediment sources at site MD95-2002 according to the palaeogeography of western Europe during the LGM (Fig. 1). Note that very unradiogenic values ($-23.3 < \varepsilon_{Nd} < -13.8$) characterise rivers draining the Baltic Shield (i.e., Scandinavia) and the southeastern Baltic rivers (i.e., North European Plain - East). ISIS: Irish Sea Ice Stream; BIIS: British-Irish Ice Sheet; SIS: Scandinavian Ice Sheet.

TABLE 3. Neodymium isotope signature of the clay-silt fraction (<63µm) of LGM glacigenic sediment samples. Measured $^{143}Nd/^{144}Nd$ ratios are reported in ε_{Nd} notation, $[(^{143}Nd/^{144}Nd)_{sample}/(^{143}Nd/^{144}Nd)_{CHUR} - 1] \times 10^4$, using $(^{143}Nd/^{144}Nd)_{CHUR} = 0.512638$ (Jacobsen and Wasserburg, 1980). Samples were collected from LGM glacial environments along the southern margins of the Irish Sea Ice Stream (ISIS), of the British-Irish (BIIS) and Scandinavian (SIS) ice-sheets and in the course of the Channel River (Fig. 1). Geographic

clusters (with mean ε_{Nd} signature) correspond to potential sediment sources at site MD95-2002 according to the palaeogeography of western Europe during the LGM (Fig. 1) [Ref. 1: O'Cofaigh and Evans (2007); 2: McCabe et al. (1990) ; 3: Clerc et al. (2012); 4: Lunkka (1988); 5: Evans and Thomson (2010); 6: Mellett et al. (2012); 7: Van Vliet-Lanöe et al. (2010); 8: Carr et al. (2006); 9: Houmark-Nielsen and Kjaer (2003) ;10: Pedersen (2005); 11: Houmark-Nielsen (1987); 12: Kabel (Kabel, 1983); 13: Lüghtens et al. (2010); 14: Lüghtens et al. (2011); 15: Weckwerth (2011); 16: Narloch et al. (2012); 17: Wysota et al. (2009); 18: Tylman et al. (Tylman et al., 2012); 19: Lesemann et al. (2010); 20: Krzyskowski et al. (1999)]. Note that the mean ε_{Nd} signature for the ISIS region (-11.8 ± 0.7) does not include the sample from Kilmore Quay (-0.6 ± 0.3). IMV: ice-marginal valleys; IMP: ice-marginal position; IA: ice advance; Fm: formation; Dmm: Diamict, matrix-supported, massive; Dms: Diamict, matrix-supported, stratified.

TABLE 4. Timing for Channel River meltwater discharges (i.e., runoff -R- events 1 to 5) and tentative correlation with the latest glacial morphostratigraphy (i.e., moraine belts, see Fig. 1) in the Baltic lowlands.

SUPPLEMENTARY TABLE S1. Neodymium isotopic composition for MD95-2002. Note that measured $^{143}Nd/^{144}Nd$ ratios are reported in ε_{Nd} notation, $[(^{143}Nd/^{144}Nd)_{sample}/(^{143}Nd/^{144}Nd)_{CHUR} - 1] \times 10^4$, using $(^{143}Nd/^{144}Nd)_{CHUR} = 0.512638$ (Jacobsen and Wasserburg, 1980).

REFERENCES

Abe-Ouchi, A., Saito, F., Kawamura, K., Raymo, M.E., Okuno, J., Takahashi, k. and Blatter, H., 2013. Insolation-driven 100,000-year glacial cycles and hysteresis of ice-sheet volume. Nature, 500: 190-194.

Alvarez-Solas, J., Charbot, S., Ritz, C., Paillard, D., Ramstein, G. and Dumas, C., 2010. Links between ocean temperature and iceberg discharge during Heinrich events. Nature Geoscience, 3: 122-126.

Alvarez-Solas, J., Robinson, A., Montoya, M. and Ritz, C., 2013. Iceberg discharges of the last glacial period driven by oceanic circulation changes. Proceedings of the National Academy of Sciences, 110(41): 16350-16354.

Andersen, K.K. et al., 2006. The Greenland Ice Core Chronology 2005, 15-42 kyr. Part 1: constructing the time scale. Quaternary Science Reviews, 25(23-24): 3246-3257.

Andrews, J.T. and Tedesco, K., 1992. Detrital carbonate-rich sediments, northwestern Labrador Sea: implications for ice-sheet dynamics and iceberg rafting (Heinrich) events in the North Atlantic. Geology, 20: 1087-1090.

Arz, H.W., Pätzold, J. and Wefer, G., 1998. Correlated millennial-scale changes in surface hydrography and terrigenous sediment yield inferred from Last-Glacial marine deposits off northeastern Brazil. Quaternary Research, 50(2): 157-166.

Auffret, G., Zaragosi, S., Dennielou, B., Cortijo, E., Van Rooij, D., Grousset, F., Pujol, C., Eynaud, F. and Siegert, M., 2002. Terrigenous fluxes at the Celtic margin during the last glacial cycle. Marine Geology, 188(1-2): 79-108.

Auffret, G.A., Boelaert, A., Vergnaud-Grazzini, C., Muller, C. and Kerbrat, R., 1996. Identification of Heinrich Layers in core KS 01 North-Eastern Atlantic (46°N, 17°W), implications for their origin. Marine Geology, 131(1-2): 5-20.

Ayliffe, L.K. et al., 2013. Rapid interhemispheric climate links via the Australasian monsoon during the last deglaciation. Nature Communications, 4: doi:10.1038/ncomms3908.

Bard, E., Rostek, F., Turon, J.L. and Gendreau, S., 2000. Hydrological impact of Heinrich events in the subtropical Northeast Atlantic. Science, 289: 1321-1324.

Barker, S., Chen, J., Gong, X., Jonkers, L., Knorr, G. and Thornalley, D., 2015. Icebergs not the trigger for North Atlantic cold events. Nature, 520: 333-338.

Barker, S. and Diz, P., 2014. Timing of the descent into the last Ice Age determined by the bipolar seesaw. Paleoceanography, 29, doi:10.1002/2014PA002623.

Barker, S., Diz, P., Vautravers, M.J., Pike, J., Knorr, G., Hall, I.R. and Broecker, W.S., 2009. Interhemispheric Atlantic seesaw response during the last deglaciation. Nature, 457: 1097-1103.

Bayon, G., Barrat, J.-A., Etoubleau, J., Benoit, M., Revillon, S. and Bollinger, C., 2009. Determination of rare earth elements, Sc, Y, Zr, Ba, Hf and Th in geological samples by ICP-MS after Tm addition and alkaline fusion. Geostandards Geoanalytical Research, 33: 51-62.

Bayon, G., Dennielou, B., Etoubleau, J., Ponzevera, E., Toucanne, S. and Bermell, S., 2012. Intensifying Weathering and Land Use in Iron Age Central Africa. Science, 335: 1219-1222.

Bayon, G., German, C.R., Boella, R.M., Mitton, J.A., Taylor, R.N. and Nesbitt, R.W., 2002. An improved method for extracting marine sediment fractions and its application to Sr and Nd isotopic analysis. Chemical Geology, 187(3-4): 179-199.

Blaauw, M., 2010. Methods and code for 'classical' age-modelling of radiocarbon sequences. Quaternary Geochronology, 5: 512-518.

Bogdanova, S.V., Bingen, B., Gorbatschev, R., Kheraskova, T.N., Klozov, V.I., Puchkov, V.N. and Volozh, Y.A., 2008. The East European Craton (Baltica) before and during the assembly of Rodania. Precambrian Research, 160(1-2): 23-45.

Bond, G., Broecker, W., Johnsen, S., McManus, J., Labeyrie, L., Jouzel, J. and Bonani, G., 1993. Correlations between climate records from North Atlantic sediments and Greenland ice. Nature, 365: 143-147.

Bond, G. and Lotti, R., 1995. Iceberg Discharges into the North Atlantic on Millennial Time Scales During the Last Glaciation. Science, 267: 1005-1010.

Böse, M., Lüghtens, C., Lee, J.R. and Rose, J., 2012. Quaternary glaciations of northern Europe. Quaternary Science Reviews, 44: 1-25.

Boulton, G. and Hagdorn, M., 2006. Glaciology of the British Isles Ice Sheet during the last glacial cycle: form, flow, streams and lobes. Quaternary Science Reviews, 25(23-24): 3359-3390.

Boulton, G.S., Dongelmans, P., Punkari, M. and Broadgate, M., 2001. Paleoglaciology of an ice sheet through a glacial cycle: the European ice sheet through the Weichselian. Quaternary Science Reviews, 20: 591-625.

Boulton, G.S., Smith, G.D., Jones, A.S. and Newsome, J., 1985. Glacial geology and glaciology of the last mid-latitude ice sheets. Journal of the Geological Society, London, 142: 447-474.

Bourillet, J.F., Reynaud, J.Y., Baltzer, A. and Zaragosi, S., 2003. The "Fleuve Manche": the submarine sedimentary features from the outer shelf to the deep-sea fans. Journal of Quaternary Science, 18(3-4): 261-282.

Bradwell, T. et al., 2008. The northern sector of the last British Ice Sheet: Maximum extent and demise. Earth-Science Reviews, 88(3-4): 207-226.

Broecker, W.S., 2006. Was the Younger Dryas triggered by a flood? Science, 312: 1146-1148.

Broecker, W.S., Andree, M., Wolfli, W., Oeschger, H., Bonani, G. and Kennett, J., 1988. The chronology of the last deglaciation: Implications to the cause of the Younger Dryas event. Paleoceanography, 3(1): 1-19.

Brown, P.A. and Kennett, J.P., 1998. Megaflood erosion and meltwater plumbing changes during last North American deglaciation recorded in Gulf of Mexico sediments. Geology, 26: 599-602.

Busschers, F.S. et al., 2007. Late Pleistocene evolution of the Rhine-Meuse system in the southern North-Sea Basin: Imprints of climate change, sea-level oscillation and glacio-isostacy. Quaternary Science Reviews, 26(25-28): 3216-3248.

Carlson, A.E. and Clark, P.U., 2012. Ice sheet sources of sea level rise and freshwater discharge during the last deglaciation. Reviews of Geophysics, 50: RG4007, doi:10.1029/2011RG000371.

Carlson, A.E., Clark, P.U., Haley, B.A., Klinkhammer, G.P., Simmons, K., Brook, E.J. and Meissner, K.J., 2007. Geochemical proxies of North American freshwater routing during the Younger Dryas cold event. Proceedings of the National Academy of Sciences of the United States of America, 104(16): 6556-6561.

Carlson, A.E., Oppo, D.W., Came, R.E., LeGrande, A.N., Keigwin, L.D. and Curry, W.B., 2008. Subtropical Atlantic salinity variability and Atlantic meridional circulation during the last deglaciation. Geology, 36: 991-994.

Carlson, A.E. and Winsor, K., 2012. Northern Hemisphere ice-sheet responses to past climate warming. Nature Geoscience, 5(9): 607-613.

Carr, S.J., Haflidason, H. and Sejrup, H.P., 2000. Micromorphological evidence supporting Late Weichselian glaciation of the northern North Sea. Boreas, 29: 315-328.

Carr, S.J., Holmes, R., Van der Meer, J.J.M. and Rose, J., 2006. The Last Glacial Maximum in the North Sea Basin: micromorphological evidence of extensive glaciation. Journal of Quaternary Science, 21(2): 131-153.
Cheng, H., Edwards, R.L., Broecker, W.S., Denton, G.H., Kong, X., Wang, Y., Zhang, R. and Wang, X., 2009. Ice Age Terminations. Science, 326: 248-252.
Chiverrell, R.C. et al., 2013. Bayesian modelling the retreat of the Irish Sea Ice Stream. Journal of Quaternary Science, 28(2): 200-209.
Clark, C.D., Gibbard, P. and Rose, J., 2004a. Pleistocene glacial limits in England, Scotland and Wales. In: Ehlers, J., Gibbard, P.L. (Eds.): Quaternary Glaciations: Extent and Chronology, Vol. 1, Europe. Developments in Quaternary Science. Elsevier, Oxford.: 47-82.
Clark, C.D., Hughes, A.L.C., Greenwood, S.L., Jordan, C. and Sejrup, H.S., 2012a. Pattern and timing of retreat of the last British-Irish Ice Sheet. Quaternary Science Reviews, 44: 112-146.
Clark, J., McCabe, A.M., Bowen, D.Q. and Clark, P.U., 2012b. Response of the Irish Ice sheet to abrupt climate change during the last deglaciation. Quaternary Science Reviews, 35: 100-115.
Clark, P.U. and Bartlein, P.J., 1995. Correlation of late Pleistocene glaciation in the western United States with North Atlantic Heinrich events. Geology, 23(6): 483-486.
Clark, P.U., Dyke, A.S., Shakun, J.D., Carlson, A.E., Clark, J., Wohlfarth, B., Mitrovica, J.X., Hostetler, S.W. and McCabe, A.M., 2009. The Last Glacial Maximum. Science, 325: 710-714.
Clark, P.U., Hostetler, S.W., Pisias, N.G., Schmittner, A. and Meissner, K.J., 2007. Mechanisms for an ~7-Kyr Climate and Sea-Level Oscillation During Marine Isotope Stage 3, in Ocean Circulation: Mechanisms and Impacts - Past and Future Changes of Meridional Overturning (eds A. Schmittner, J. C. H. Chiang and S. R. Hemming), American Geophysical Union, Washington, D. C. doi: 10.1029/173GM15.
Clark, P.U., Marshall, S.J., Clarke, G.K.C., Hostetler, S.W., Licciardi, J.M. and Teller, J.T., 2001. Freshwater forcing of abrupt climate change during the last glaciation. Science, 293(5528): 283-287.
Clark, P.U., McCabe, A.M., Mix, A.C. and Weaver, A.J., 2004b. Rapid sea level rise at 19,000 years ago and its global implications. Science, 304: 1141-1144, doi: 10.1126/science.1094449.
Clark, P.U. et al., 2012c. Global climate evolution during the last deglaciation. Proceedings of the National Academy of Sciences, 109(19): E1134-E1142.
Clerc, S., Buoncristiani, J.F., Guiraud, M., Desaubliaux, G. and Portier, E., 2012. Depositional model in subglacial cavities, Killiney Bay, Ireland. Interactions between sedimentation, deformation and glacial dynamics. Quaternary Science Reviews, 33: 142-164.
Curry, B. and Petras, J., 2011. Chronological framework for the deglaciation of the Lake Michigan lobe of the Laurentide Ice Sheet from ice-walled lake deposits. Journal of Quaternary Science, 26: 402-410.
Davies, G., Gledhill, A. and Hawkesworth, C., 1985. Upper crustal recycling in southern Britain: evidence from Nd and Sr isotopes. Earth and Planetary Science Letters, 75: 1-12.
Denton, G.H., Alley, R.B., Comer, G.C. and Broecker, W.S., 2005. The role of seasonality in abrupt climate change. Quaternary Science Reviews, 24(10-11): 1159-1182.
Denton, G.H., Anderson, R.F., Toggweiler, J.R., Edwards, R.L., Schaefer, J.M. and Putnam, A.E., 2010. The Last Glacial Termination. Science, 328: 1652-1656.

Denton, G.H., Heusser, C.J., Lowell, T.V., Schlüchter, C., Andersen, B.G., Heusser, L.E., Moreno, P.I. and Marchant, D.R., 1999. Geomorphology, Stratigraphy, and Radiocarbon Chronology of Llanquihue Drift in the Area of the Southern Lake District, Seno Reloncaví, and Isla Grande de Chiloé, Chile. Geografiska Annaler. Series A, Physical Geography, 81(2): 167-229.

Duan, F., Wu, J., Wang, Y., Edwards, R.L., Cheng, H., Kong, X. and Zhang, W., 2015. A 3000-yr annually laminated stalagmite record of the Last Glacial Maximum from Hulu Cave, China. Quaternary Research, 83(2): 360-369.

Ehlers, J., Gibbard, P.L. and Hughes, P.D., 2011a. Quaternary Glaciations - Extent and Chronology, 15. Elsevier, Amsterdam, 1126 pp.

Ehlers, J., Grube, A., Stephan, H.-J. and Wansa, S., 2011b. Pleistocene glaciations of North Germany-New results, in Ehlers J., Gibbard P.L., Hughes P.D., eds., Quaternary Glaciations: Extent and Chronology-A Closer Look: Developments in Quaternary Science, v. 15, p. 149-162.

Evans, D.J.A. and Thomson, S.A., 2010. Glacial sediments and landforms of Holderness, eastern England: a glacial depositional model for the North Sea Lobe of the British-Irish Ice Sheet. Earth Science Reviews, 101: 147-189.

Eynaud, F., 1999. Dinoflagellate cyst countings of sediment core MD95-2002, doi:10.1594/PANGAEA.94355.

Eynaud, F. et al., 2009. Position of the Polar Front along the western Iberian margin during key cold episodes of the last 45 ka. Geochemistry, Geophysics, Geosystems, 10, Q07U05, doi:10.1029/2009GC002398.

Eynaud, F. et al., 2012. New constraints on European glacial freshwater releases to the North Atlantic Ocean. Geophysical Research Letters, 39(15): doi:10.1029/2012GL052100.

Eynaud, F., Zaragosi, S., Scourse, J.D., Mojtahid, M., Bourillet, J.F., Hall, I.R., Penaud, A., Locascio, M. and Reijonen, A., 2007. Deglacial laminated facies on the NW European continental margin: the hydrographic significance of British Ice sheet deglaciation and Fleuve Manche paleoriver discharges. Geochemistry, Geophysics, Geosystems, 8, doi:10.1029/2006GC001496.

Freslon, N. et al., 2014. Rare earth elements and neodymium isotopes in sedimentary organic matter. Geochimica et Cosmochimica Acta, 140: 177-198.

Ganopolski, A. and Rahmstorf, S., 2001. Rapid changes of glacial climate simulated in a coupled climate model. Nature, 409(6817): 153-158.

Gibbard, P.L., 1988. The history of great northwest European rivers during the past three millions years. Phil. Trans. R. Soc. Lond., B318: 559-602.

Goldstein, S.J. and Jacobsen, S.B., 1987. The Nd and Sr isotopic systematics of river-water dissolved material: Implications for the sources of Nd and Sr in the seawater. Chemical Geology, 66: 245- 272.

Goldstein, S.J. and Jacobsen, S.B., 1988. Nd and Sr isotopic systematics of river-water suspended material: Implications for crustal evolution. Earth and Planetary Science Letters, 87: 249- 265.

Goldstein, S.L., O'Nions, R.K. and Hamilton, P.J., 1984. A Sm-Nd study of atmospheric dusts and particulate from major river systems. Earth and Planetary Science Letters, 70: 221-236.

Graham, A.G.C., Lonergan, L. and Stoker, M., 2010. Depositional environments and chronology of Late Weichselian glaciation and deglaciation in the central North Sea. Boreas, 39(3): 471-491.

Grousset, F.E., Pujol, C., Labeyrie, L., Auffret, G. and Boelaert, A., 2000. Were the North Atlantic Heinrich events triggered by the behavior of the European ice sheets? Geology, 28(2): 123-126.

Gupta, S., Collier, J.S., Palmer-Felgate, A. and Potter, G., 2007. Catastrophic flooding origin of shelf valley systems in the English Channel. Nature, 448(7151): 342-345.

Hall, B.L., Porter, C.T., Denton, G.H., Lowell, T.V. and Bromley, G.R.M., 2013. Extensive recession of Cordillera Darwin glaciers in southernmost South America during Heinrich Stadial 1. Quaternary Science Reviews, 62: 49-55.

Hall, I.R., Colmenero-Hidalgo, E., Zahn, R., Peck, V.L. and Hemming, S.R., 2011. Centennial- to millenial-scale ice-ocean interactions in the subpolar northeast atlantic 18-41 kyr ago. Paleoceanography, PA2224, 26.

Hall, I.R., Moran, S.B., Zahn, R., Knutz, P.C., Shen, C.C. and Edwards, R.L., 2006. Accelerated drawdown of meridional overturning in the late-glacial Atlantic triggered by transient pre-H event freshwater perturbation. Geophysical Research Letters, 33(16): L16616, doi:10.1029/2006GL026239.

Heine, K., Reuther, A.U., Thieke, H.U., Schulz, R., Schlaak, N. and Kubik, P.W., 2009. Timing of Weichselian ice marginal positions in Brandenburg (northeastern Germany) using cosmogenic *in situ* ^{10}Be. Zeitschrift für Geomorphologie, 53: 433-454.

Hemming, S.R., 2004. Heinrich events: Massive late Pleistocene detritus layers of the North Atlantic and their global climate imprint. Reviews of Geophysics, 42(1): RG1005 1-43.

Heyman, J., Stroeven, A.P., Harbor, J.M. and Caffee, M.W., 2011. Too young or too old: Evaluating cosmogenic exposure dating based on an analysis of compiled boulder exposure ages. Earth and Planetary Science Letters, 302: 71-80.

Hopmans, E.C., Weijers, J.W.H., Schefuß, E., Herfort, L., Sinninghe Damsté, J.S. and Schouten, S., 2004. A novel proxy for terrestrial organic matter in sediments based on branched and isoprenoid tetraether lipids. Earth and Planetary Science Letters, 224(1-2): 107-116.

Houmark-Nielsen, M., 1987. Pleistocene stratigraphy and glacial history of the central part of Denmark. Bulletin of the Geological Society of Denmark, 36: 1-189.

Houmark-Nielsen, M., 2003. Signature and timing of the Kattegat Ice Stream: onset of the Last Glacial Maximum sequence at the southwestern margin of the Scandinavian Ice Sheet. Boreas, 32(1): 227-241.

Houmark-Nielsen, M., 2010. Extent, age and dynamics of Marine Isotope Stage 3 glaciations in the southwestern Baltic Basin. Boreas, 39(2): 343-359.

Houmark-Nielsen, M., Björck, S. and Wohlfarth, B., 2006. 'Cosmogenic ^{10}Be ages on the Pomeranian Moraine, Poland': Comments. Boreas, 35.

Houmark-Nielsen, M. and Kjær, K.H., 2003. Southwest Scandinavia, 40-15 kyr BP: palaeogeography and environmental change. Journal of Quaternary Science, 18(8): 769-786.

Houmark-Nielsen, M., Linge, H., Fabel, D., Schnabel, C., Xu, S., Wilcken, K.M. and Binnie, S., 2012. Cosmogenic surface exposure dating the last deglaciation in Denmark: Discrepancies with independant age constraints suggest delayed periglacial landform stabilisation. Quaternary Geochronology, 13: 1-17.

Hubbard, A., Bradwell, T., Golledge, N., Hall, A., Patton, H., Sugden, D., Cooper, R. and Stoker, M., 2009. Dynamic cycles, ice streams and their impact on the extent, chronology and deglaciation of the British-Irish ice sheet. Quaternary Science Reviews, 28(7-8): 758-776.

Huybers, P., 2006. Early Pleistocene glacial cycles and the integrated summer insolation forcing. Science, 313: 508-511.

Jacobsen, S.B. and Wasserburg, G.J., 1980. Sm-Nd isotopic evolution of chondrites. Earth and Planetary Science Letters, 50: 139-155.

Jennerjahn, T.C., Ittekkot, V., Arz, H.W., Behling, H., Patzold, J. and Wefer, G., 2004. Asynchronous Terrestrial and Marine Signals of Climate Change during Heinrich Events. Science, 306: 2236-2239.

Kabel, C., 1983. The Brodtener Ufer Cliff. In Ehlers, J. (Eds), Glacial deposits in North-West Europe. Rotterdam, Balkema, 325-327.

Kadereit, A., Kind, C.J. and Wagner, G.A., 2013. The chronological position of the Lohne Soil in the Nußloch loess section - re-evaluation for a European loess-marker horizon. Quaternary Science Reviews, 59: 67-86.

Kjær, K.H., Houmark-Nielsen, M. and Richardt, N., 2003. Ice-flow patterns and dispersal of erratics at the southwestern margin of the last Scandinavian Ice Sheet: signature of palaeo-ice streams. Boreas, 32: 130-148.

Knutz, P.C., Zahn, R. and Hall, I.R., 2007. Centennial-scale variability of the British Ice Sheet: Implications for climate forcing and Atlantic meridional overturning circulation during the last deglaciation. Paleoceanography, 22(1): PA1207/doi:10.1029/2006PA001298

Krzyszkowski, D., Gizler, H., Jodlowski, J. and Dobosz, T., 1999. Quaternary geology and geomorphology in the zone of the maximum extent of the Weichselian ice sheet between Slawa slaska and Swieciechowa, western Poland. Quaternary studies in Poland, 16: 47-66.

Larsen, N.K., Knudsen, K.L., Krohn, C.F., Kronborg, C., Murray, A.S. and Nielsen, O.B., 2009. Late Quaternary ice sheet, lake and sea history of southwest Scandinavia - a synthesis. Boreas, 38(4): 732-761.

Laskar, J., Robutel, P., Joutel, F., Gastineau, M., Correia, A.C.M. and Levrard, B., 2004. A long-term numerical solution for the insolation quantities of the Earth. Astronomy and Astrophysics, 428(1): 261-285.

Lehman, S.J., Jones, A.G., Keigwin, L.D., Andersen, E.S., Butenko, G. and Ostmo, S.R., 1991. Initiation of Fennoscandian ice-sheet retreat during the last deglaciation. Nature, 349: 513-516.

Lekens, W.A.H., Sejrup, H.P., Haflidason, H., Knies , J. and Richter, T., 2006. Meltwater and ice rafting in the southern Norwegian Sea between 20 to 40 calendar kyr B.P.: Implications for Fennoscandian Heinrich events. Palaeoceanography, 21: doi:10.1029/2005PA001228.

Lesemann, J.E., Piotrowski, J.A. and Wysota, W., 2010. Glacial curvilineations: New glacial landforms produced by longitudinal vortices in subglacial meltwater flows. Geomorphology, 120(3-4): 153-161.

Levine, R.C. and Bigg, G.R., 2008. Sensitivity of the glacial ocean to Heinrich events from different iceberg sources, as modeled by a coupled atmosphere-iceberg-ocean model. Paleoceanography, 23, doi:10.1029/2008PA001613.

Litt, T., Behre, K.-E., Meyer, K.-D., Stephan, H.-J. and Wansa, S., 2007. Stratigraphishe Begriffe für das Quartär des norddeutschland Vereisungsgebietes. Quaternary Science Journal, 56: 7-65.

Lopes, C. and Mix, A.C., 2009. Pleistocene megafloods in the northeast Pacific. Geology, 37: 79-82.

Lüghtens, C. and Böse, M., 2011. Chronology of Weichselian main ice marginal positions in north-eastern Germany. Quaternary Science Journal, 60(2-3): 236-247.

Lüghtens, C., Böse, M. and Preusser, F., 2011. Age of the Pomeranian ice-marginal position in northeastern Germany determined by Optically Stimulated Luminescence (OSL) dating of glaciofluvial sediments. Boreas, 40(4): 598-615.

Lüghtens, C., Krbetschek, M., Böse, M. and Fuchs, M.C., 2010. Optically stimulated luminescence dating of fluvioglacial (sandur) sediments from north-eastern Germany. Quaternary Geochronology, 5: 237-243.

Lunkka, J.P., 1988. Sedimentation and deformation of the North Sea Droft formation in the Happisburg area, North Norfolk. . In Groot, David G. (ed.) Glaciotectonics Forms and Processes. Balkema, Rotterdam, pp.109-122.

Mangerud, J., Gulliksen, S. and Larsen, E., 2010. ^{14}C-dated fluctuations of the western flank of the Scandinavian Ice Sheet 45-25 kyr BP compared with Bølling-Younger Dryas fluctuations and Dansgaard-Oeschger events in Greenland. Boreas, 39(2): 328-342.

Marcott, S.A. et al., 2011. Ice-shelf collapse from subsurface warming as a trigger for Heinrich events. Proceedings of the National Academy of Sciences, 108(33): 13415-13419.

Marks, L., 2002. Last Glacial Maximum in Poland. Quaternary Science Reviews, 21(1-3): 103-110.

Marks, L., 2012. Timing of Late Vistulian (Weichselian) glacial phases in Poland. Quaternary Science Reviews, 44: 81-88.

McCabe, A.M. and Clark, P.U., 1998. Ice-sheet variability around the North Atlantic Ocean during the last deglaciation. Nature, 392: 373-376.

McCabe, A.M., Clark, P.U. and Clark, J., 2007. Radiocarbon constraints on the history of the western Irish ice sheet prior to the Last Glacial Maximum. Geology, 35(2): 147-150.

McCabe, A.M., Eyles, N., Haynes, J.R. and Bowen, D.Q., 1990. Biofacies and sediments in an emergent Late Pleistocene glaciimarine sequence, Skerries, east central Ireland. Marine Geology, 94: 23-26.

McManus, J.F., Francois, R., Gherardi, J.M., Keigwin, L.D. and Drown-Leger, S., 2004. Collapse and rapid resumption of Atlantic meridional circulation linked to deglacial climate changes. Nature, 428(6985): 834-837.

Mellett, C.L., Mauz, B., Plater, A.J., Hodgson, D.M. and Lang, A., 2012. Optical dating of drowned landscapes: A case study from the English Channel. Quaternary Geochronology, 10: 201-208.

Ménot, G., Bard, E., Rostek, F., Weijers, J.W.H., Hopmans, E.C., Schouten, S. and Sinninghe Damsté, J.S., 2006. Early reactivation of European Rivers during the last deglaciation. Science, 313: 1623-1625.

Michard, A., Gurret, P., Soudant, M. and Albarède, F., 1985. Nd isotopes in French Phanerozoic shales: external vs. internal aspects of crustal evolution. Geochimica et Cosmochimica Acta, 49: 601-610.

Mojtahid, M., Eynaud, F., Zaragosi, S., Scourse, J., Bourillet, J.F. and Garlan, T., 2005. Palaeoclimatology and palaeohydrography of the glacial stages on Celtic and Armorican margins over the last 360 000 yrs. Marine Geology, 224(1-4): 57-82.

Möller, P. and Murray, A.S., 2015. Drumlinised glaciofluvial and glaciolacustrine sediments on the Småland peneplain, South Sweden – new information on the growth and decay history of the Fennoscandian Ice Sheets during MIS 3. Quaternary Science Reviews, 122: 1-29.

Murray, D.S., Carlson, A.E., Singer, B.S., Anslow, F.S., He, F., Caffee, M., Marcott, S.A., Liu, Z. and Otto-Bliesner, B.L., 2012. Northern Hemisphere forcing of the last deglaciation in southern Patagonia. Geology, 40(7): 631-634.

Narloch, W., Piotrowski, J.A., Wysota, W., Larsen, N.K. and Menzies, J., 2012. The signature of strain magnitude in tills associated with the Vistula Ice Stream of the Scandinavian Ice Sheet, central Poland. Quaternary Science Reviews, 57: 105-120.

NGRIP-members, 2004. High resolution climate record of the northern hemisphere reaching into the last interglacial period. Nature, 431: 147-151.

Nygard, A., Sejrup, H.P., Haflidason, H., Cecchi, M. and Ottesen, D., 2004. Deglaciation history of the southwestern Fennoscandian Ice Sheet between 15 and 13 ^{14}C ka BP. Boreas, 33: 1-17.

O'Cofaigh, C. and Evans, D.J.A., 2007. Radiocarbon constraints on the age of the maximum advance of the British-Irish Ice Sheet in the Celtic Sea. Quaternary Science Reviews, 26(9-10): 1197-1203.

O´Cofaigh, C. and Evans, D.J.A., 2001. Sedimentary evidence for deforming bed conditions associated with a grounded Irish Sea Glacier, southern Ireland. Journal of Quaternary Science, 16: 435-454.

Paillard, D., 2015. Quaternary glaciations: from observations to theories. Quaternary Science Reviews, 107: 11-24.

Peck, V.L., Hall, I.R., Zahn, R., Elderfield, H., Grousset, F., Hemming, S.R. and Scourse, J.D., 2006. High resolution evidence for linkages between NW European ice sheet instability and Atlantic Meridional Overturning Circulation. Earth and Planetary Science Letters, 243(3-4): 476-488.

Peck, V.L., Hall, I.R., Zahn, R. and Scourse, J.D., 2007. Progressive reduction in NE Atlantic intermediate water ventilation prior to Heinrich events: Response to NW European ice sheet instabilities. Geochemistry, Geophysics, Geosystems, 8, doi: 10.1029:2006GC001321.

Pedersen, S.A.S., 2005. Structural analysis of the Rubjerg Knude Glaciotectonic Complex, Vendsyssel, northern Denmark. Geological Survey of Denmark and Greenland Bulletin, 8: 1-192.

Peucker-Ehrenbrink, B., Miller, M.W., Arsouze, T. and Jeandel, C., 2010. Continental bedrock and riverine fluxes of strontium and neodymium isotopes to the oceans. Geochemistry, Geophysics, Geosystems, 11, Q03016, doi:10.1029/2009GC002869.

Praetorius, S.K., McManus, J.F., Oppo, D.W. and Curry, W.B., 2008. Episodic reductions in bottom-water currents since the last ice age. Nature Geoscience, 1: 449-452.

Putnam, A.E. et al., 2013. Warming and glacier recession in the Rakaia valley, Southern Alps of New Zealand, during Heinrich Stadial 1. Earth and Planetary Science Letters, 382: 98-110.

Rahmstorf, S., 1995. Bifurcations of the Atlantic thermohaline circulation in response to changes in the hydrological cycle. Nature, 378(6554): 145-149.

Rasmussen, S.O. et al., 2006. A new Greenland ice core chronology for the last glacial termination. Journal of Geophysical Research, 111, D06102, doi:10.1029/2005JD006079.

Reimer, P.J. et al., 2013. Intcal13 and Marine13 radiocarbon age calibration curves 0-50,000 years cal BP. Radiocarbon, 55(4): 1869-1887.

Richter, T.O., Van Der Gaast, S., Koster, B., Vaars, A., Gieles, R., De Stigter, H.C., De Haas, H. and Van Weering, T.C.E., 2006. The Avaatech XRF Core Scanner: technical description and applications to NE Atlantic sediments. In: R.G. Rothwell (Editor), New Techniques in Sediment Core Analysis. Geological Society, Special Publications, pp. 39-50.

Ridge, J.C., Balco, G., Bayless, R.L., Beck, C.C., Carter, L.B., Dean, J.L., Voytek, E.B. and Wei, J.H., 2012. The new North American varve chronology: A precise record of southeastern Laurentide Ice Sheet deglaciation and climate, 18.2-12.5 kyr BP, and correlations with Greenland ice core records. American Journal of Science, 312(7): 685-722.

Rinterknecht, V., Börner, A., Bourlès, D. and Braucher, R., 2013. Cosmogenic ^{10}Be dating of ice sheet marginal belts in Mecklenburg-Vorpommern, Western Pomerania (northeast Germany). Quaternary Geochronology, 19: 42-51.

Rinterknecht, V., Braucher, R., Böse, M., Bourlès, D. and Mercier, J.L., 2012. Late Quaternary ice sheet extents in northeastern Germany inferred from surface exposure dating. Quaternary Science Reviews, 44: 89-95.

Rinterknecht, V.R. et al., 2006. The last deglaciation of the southeastern sector of the Scandinavian ice sheet. Science, 311(5766): 1449-1452.

Rinterknecht, V.R., Marks, L., Piotrowski, J.A., Raisbeck, G.M., Yiou, F., Brook, E.J. and Clark, P.U., 2005. Cosmogenic ^{10}Be ages on the Pomeranian Moraine, Poland. Boreas, 34: 186-191.

Rinterknecht, V.R., Pavlovskaya, I.E., Clark, P.U., Raisbeck, G.M., Yiou, F. and Brook, E.J., 2007. Timing of the last deglaciation in Belarus. Boreas, 36: 307-313.

Roche, D., Wiersma, A.P. and Renssen, H., 2010. A systematic study of the impact of freshwater pulses with respect to different geographical locations. Climate Dynamics, 34(7): 997-1013.

Rochon, A., de Vernal, A., Turon, J.L., Matthiessen, J. and Head, M.J., 1999. Recent dinoflagellate cysts of the North Atlantic Ocean and adjacent seas in relation to sea-surface parameters. AASP Contribution Serie, 35: 1-152.

Rühlemann, C., Mulitza, S., Müller, P.J., Wefer, G. and Zahn, R., 1999. Warming of the tropical Atlantic Ocean and slowdown of thermohaline circulation during the last deglaciation. Nature, 402: 511-514.

Scourse, J.D., Haapaniemi, A.I., Colmenero-Hidalgo, E., Peck, V.L., Hall, I.R., Austin, W.E.N., Knutz, P.C. and Zahn, R., 2009. Growth, dynamics and deglaciation of the last British-Irish ice sheet: the deep-sea ice-rafted detritus record. Quaternary Science Reviews, 28: 3066-3084.

Scourse, J.D., Hall, I.R., McCave, I.N., Young, J.R. and Sugdon, C., 2000. The origin of Heinrich layers: evidence from H2 for European precursor events. Earth and Planetary Science Letters, 182(2): 187-195.

Sejrup, H.P., Haflidason, H., Aarseth, I., King, E., Forsberg, C.F., Long, D. and Rokoengen, K., 1994. Late Weichselian glaciation history of the northern North Sea. Boreas, 23: 1-13.

Sejrup, H.P., Larsen, E., Landvik, J., King, E.L., Haflidason, H. and Nesje, A., 2000. Quaternary glaciations in southern Fennoscandia: evidence from southwestern Norway and the northern North Sea region. Quaternary Science Reviews, 19: 667-685.

Sejrup, H.P., Nygård, A., Hall, A.M. and Haflidason, H., 2009. Middle and Late Weichselian (Devensian) glaciation history of south-western Norway, North Sea and eastern UK. Quaternary Science Reviews, 28(3-4): 370-380.

Shakun, J.D., Clark, P.U., He, F., Marcott, S.A., Mix, A.C., Liu, Z., Otto-Bliesner, B., Schmittner, A. and Bard, E., 2012. Global warming preceded by increasing carbon dioxide concentrations during the last deglaciation. Nature, 484: 49-55.

Soulet, G., Ménot, G., Bayon, G., Rostek, F., Ponzevera, E., Toucanne, S., Lericolais, G. and Bard, E., 2013. Abrupt drainage cycles of the Fennoscandian Ice Sheet. Proceedings of the National Academy of Sciences, 110(17): 6682-6687.

Spötl, C., Reimer, P.J., Starnberger, R. and Reimer, R.W., 2013. A new radiocarbon chronology of Baumkirchen, stratotype for the onset of the Upper Würmian in the Alps. Journal of Quaternary Science, 28(6): 552-558.

Stern, J.V. and Lisiecki, L.E., 2013. North Atlantic circulation and reservoir age changes over the past 41,000 years. Geophysical Research Letters, 40: 3693-3697.

Toucanne, S., 2008. Reconstruction des transferts sédimentaires en provenance du système glaciaire de Mer d'Irlande et du paléofleuve Manche au cours des derniers cycles climatiques. Unpublished PhD thesis, University Bordeaux 1, n°3699, pp. 340.

Toucanne, S. et al., 2009a. Timing of massive 'Fleuve Manche' discharges over the last 350 kyr: insights into the European Ice Sheet oscillations and the European drainage network from MIS 10 to 2. Quaternary Science Reviews, 28(13-14): 1238-1256.

Toucanne, S., Zaragosi, S., Bourillet, J.F., Dennielou, B., Jorry, S.J., Jouet, G. and Cremer, M., 2012. External controls on turbidite sedimentation on the glacially-influenced Armorican margin (Bay of Biscay, western European margin). Marine Geology, 303-306: 137-153.

Toucanne, S. et al., 2009b. A 1.2 My record of glaciation and fluvial discharges from the West European Atlantic margin. Quaternary Science Reviews, 28: 2974-2981.

Toucanne, S. et al., 2010. The first estimation of Fleuve Manche palaeoriver discharge during the last deglaciation: Evidence for Fennoscandian ice sheet meltwater flow in the English Channel ca 20-18 ka ago. Earth and Planetary Science Letters, 290: 459-473.

Toucanne, S., Zaragosi, S., Bourillet, J.F., Naughton, F., Cremer, M., Eynaud, F. and Dennielou, B., 2008. Activity of the turbidite levees of the Celtic-Armorican margin (Bay of Biscay) during the last 30,000 years: Imprints of the last European deglaciation and Heinrich events. Marine Geology, 247(1-2): 84-103.

Tylman, K., Piotrowski, J.A. and Wysota, W., 2012. The ice/bed interface mosaic: deforming spots intervening with stable areas under the fringe of the Scandinavian Ice Sheet at Samplawa, Poland. Boreas, 42(2): 428-441.

Ullman, D.J., Carlson, A.E., LeGrande, A.N., Anslow, F.S., Moore, A.K., Caffee, M., Syverson, K.M. and Licciardi, J.M., 2015. Southern Laurentide ice-sheet retreat synchronous with rising boreal summer insolation. Geology, 43(1): 23-26.

Ūsaityte, D., 2000. The geology of the southeastern Baltic Sea: a review. Earth Science Reviews, 50: 137-225.

Van Vliet-Lanoë, B., Gosselin, G., Mansy, J.L., Bourdillon, C., Meurisse-Fort, M., Henriet, J.P., Le Roy, P. and Trentesaux, A., 2010. A renewed cenozoic story of the Strait of Dover. Annales de la Société Géologique du Nord, 17(2): 59-80.

WAIS-Divide-Project-members, 2013. Onset of deglacial warming in West Antarctica driven by local orbital forcing. Nature, 500: 440-444.

Wang, Y.J., Cheng, H., Edwards, R.L., An, Z.S., Wu, J.Y., Shen, C.C. and Dorale, J.A., 2001. A high-resolution absolute-dated late Pleistocene monsoon record from Hulu Cave, China. Science, 294(5550): 2345-2348.

Weber, M.E. et al., 2014. Millenial-scale variability in Antarctic ice-sheet discharge during the last deglaciation. Nature, 510: 134-138.

Weckwerth, P., 2011. Evolution of the Torun Basin in the Late Weichselian. Landform Analysis, 14: 57-84.

Wysota, W., Molewski, P. and Sokolowski, R.J., 2009. Record of the Vistula ice lobes in the Late Weichselian glacial sequence in north-central Poland. Quaternary International, 207(1-2): 26-41.

Yokoyama, Y., Lambeck, K., De Deckker, P., Johnston, P. and Fifield, L.K., 2000. Timing of the Last Glacial Maximum from observed sea-level minima. Nature, 406: 713-716.

Zaragosi, S., Bourillet, J.F., Eynaud, F., Toucanne, S., Denhard, B., Van Toer, A. and Lanfumey, V., 2006. The impact of the last European deglaciation on the deep-sea turbidite systems of the Celtic-Armorican margin (Bay of Biscay). Geo-Marine Letters, 26(6): 317-329.

Zaragosi, S., Eynaud, F., Pujol, C., Auffret, G.A., Turon, J.L. and Garlan, T., 2001. Initiation of the European deglaciation as recorded in the northwestern Bay of Biscay slope environments (Meriadzek Terrace and Trevelyan Escarpment): a multi-proxy approach. Earth and Planetary Science Letters, 188(3-4): 493-507.

Ziegler, M., Simon, M.H., Hall, I.R., Barker, S., Stringer, C. and Zahn, R., 2013. Development of Middle Stone Age innovation linked to rapid climate change. Nature communications, 4, doi:10.1038/ncomms2897.

Table1

Core label	Depth (cm)	Depth in core MD95-2002 (cm)	Lab. Number	Species	^{14}C age (yr BP)	error (1σ)	Reservoir correction[a] (^{14}C yr)	error[a] (1σ)	^{14}C age corrected for reservoir[b] (^{14}C yr BP)	error[c] (1σ)	Calendar age range[d] (yr BP, 2σ)	Ref.
MD95-2002	0	0	LSCE-99360	*G. bull*	2060	70	400	200	1660	212	1221 - 2061	1
MD95-2002	140	140	LSCE-99361	*G. bull*	9480	90	400	200	9080	219	9556 - 10761	1
NGRIP-YD/PB	-	195-205	-	-	-	-	-	-	-	-	11555 - 11750	2
MD95-2002	240	240	LSCE-99362	*N. pch(s)*	11190	100	875	200	10315	224	11390 - 12664	1
MD03-2690	626	371-379	SacA-003234	*G. bull*	13020	60	680	200	12340	209	13793 - 15129	3
NGRIP-GI1	-	380-390	-	-	-	-	-	-	-	-	14460 - 14823	2
MD03-2690	692	389-397	SacA-003235	*N. pch(s)*	13170	70	680	200	12490	212	13978 - 15367	3
MD95-2002	420	420	LSCE-99363	*N. pch(s)*	13730	130	970	200	12760	239	14227 - 15878	1
MD95-2002	454	454	LSCE-99364	*N. pch(s)*	14200	110	970	200	13230	228	15234 - 16524	1
MD95-2002	463	463	LSCE-99365	*N. pch(s)*	14420	120	970	200	13450	233	15566 - 16946	1
MD95-2002	510	510	LSCE-99366	*N. pch(s)*	14570	130	970	200	13600	239	17771 - 17121	1
MD95-2002	550	550	SacA-003242	*N. pch(s)*	14830	70	970	200	13860	212	16215 - 17411	3
MD95-2002	580	580	Beta-141702	*N. pch(s)*	14810	200	970	200	13840	283	16027 - 17545	1
MD95-2002	869	869	SacA-003243	*N. pch(s)*	15300	70	400	200	14900	212	17653 - 18601	3
MD95-2002	875	875	SacA-003244	*N. pch(s)*	15280	160	400	200	14880	256	17547 - 18665	3
MD03-2690	2923	1210-1216	SacA-005972	*G. bull*	17390	110	400	200	16990	228	19956 - 21082	4
MD03-2692	580	1220-1225	SacA-001905	*G. bull*	17290	90	400	200	16890	219	19863 - 20933	5
MD95-2002	1320	1320	SacA-003245	*G. bull*	18850	90	400	200	18450	219	21826 - 22799	3
MD95-2002	1340	1340	SacA-003246	*G. bull*	19430	100	400	200	19030	224	22463 - 23471	3
MD95-2002	1390	1390	SacA-003247	*G. bull*	20620	80	400	200	20220	215	23827 - 24986[e]	3
NGRIP-GI2	-	1410-1415	-	-	-	-	-	-	-	-	22706 - 23873	6
MD95-2002	1424	1424	Beta-123696	*N. pch(s)*	20240	60	400	200	19840	209	23397 - 24375	7
MD95-2002	1453	1453	Beta-123698	*N. pch(s)*	20430	80	400	200	20030	215	23547 - 24607	7
MD95-2002	1464	1464	Beta-123699	*N. pch(s)*	20600	80	400	200	20200	215	23799 - 24960	7
MD95-2002	1534	1534	Beta-123697	*N. pch(s)*	22250	70	400	200	21850	212	25737 - 26571	7
NGRIP-GI3	-	1590-1593	-	-	-	-	-	-	-	-	26915 - 28544	6
MD95-2002	1610	1610	Beta-99367	*N. pch(s)*	24410	250	400	200	24010	320	27614 - 28691	8
NGRIP-GI4	-	1635	-	-	-	-	-	-	-	-	27970 - 29729	6
MD95-2002	1664	1664	Beta-99368	*N. pch(s)*	25820	230	400	200	25420	305	28841 - 30385	8
NGRIP-GI5	-	1795	-	-	-	-	-	-	-	-	31341 - 33558	6
NGRIP-GI6	-	1825	-	-	-	-	-	-	-	-	32503 - 34877	6
NGRIP-GI7	-	1855	-	-	-	-	-	-	-	-	34137 - 36723	6
NGRIP-GI8	-	1895	-	-	-	-	-	-	-	-	36750 - 39590	6
MD95-2002	1948	1948	GifA-100123	*N. pch(s)*	34320	520	400	200	33920	557	36807 - 39644	8
MD95-2002	1976	1976	GifA-100124	*N. pch(s)*	35480	520	400	200	35080	557	38583 - 40870	8

a: Reservoir correction infered from Stern et Lisieki (2013)

b: Corrected ^{14}C ages are obtained by subtracting the reservoir correction to the original ^{14}C age

c: Errors associated to the corrected ^{14}C were propagated through the quadratic sum

d: Corrected ^{14}C ages were then calibrated using the atmospheric calibration curve IntCal13 (Reimer et al., 2013)

e: ^{14}C age SacA-003247 was excluded from the age model since it is in clear age inversion

Table2

River	Country	Drainage surface (10.3km²)	Lat.	Long.	143Nd/144Nd	±	2se	εNd	±	2 sd
British Isles - West (ISIS)								*-10,8*	±	*1,0*
Shannon *	Ireland	11,93	52.689	-8.910	0,512130	±	12	-9,9	±	0,3
Lee	Ireland	1,08	51.878	-8.266	0,512033	±	12	-11,8	±	0,3
Severn	UK	9,74	51.491	-2.777	0,512026	±	11	-11,9	±	0,3
British Isles - East UK (BIIS)								*-11,6*	±	*0,9*
Humber	UK	21,70	53.715	-0.442	0,512083	±	6	-10,8	±	0,3
Ouse	UK	8,94	53.704	-0.755	0,512013	±	13	-12,2	±	0,3
Trent	UK	10,75	53.657	-0.696	0,511987	±	9	-12,7	±	0,3
Hull	UK	2,02	53.839	-0.387	0,511985	±	7	-12,7	±	0,3
English Channel (downstream part of Channel River)								*-11,5*	±	*1,3*
Couesnon	France	0,83	48.629	-1.509	0,512061	±	5	-11,2	±	0,3
Orne *	France	2,24	49.133	-0.401	0,512026	±	11	-11,9	±	0,3
Seine *	France	57,39	49.438	0.371	0,512009	±	9	-12,2	±	0,3
Somme	France	4,93	50.218	1.562	0,512242	±	13	-7,7	±	0,3
Authie	France	1,16	50.277	1.988	0,512030	±	6	-11,8	±	0,3
Schelde	Belgium	15,85	51.740	3.978	0,512056	±	15	-11,3	±	0,3
Rhine *	Netherlands	123,26	51.909	4.484	0,512033	±	13	-11,8	±	0,3
Hamble	UK	0,54	50.858	-1.312	0,512019	±	12	-12,0	±	0,3
Thames	UK	11,52	51.511	0.099	0,512291	±	11	-6,7	±	0,3
Colne	UK	0,86	51.790	0.994	0,511996	±	13	-12,5	±	0,3
North European Plain - West (southwestern SIS)								*-11,4*	±	*1,1*
Ems	Germany	13,20	53.231	7.405	0,512028	±	8	-11,9	±	0,3
Weser *	Germany	38,34	53.539	8.572	0,512178	±	9	-8,9	±	0,3
Elbe *	Germany	121,21	53.703	9.449	0,512058	±	9	-11,3	±	0,3
Varde	Denmark	1,12	55.632	8.507	0,512025	±	7	-11,9	±	0,3
Oder	Germany	101,49	53.841	14.121	0,512003	±	13	-12,4	±	1,3
North European Plain - East (southeastern SIS)								*-14,8*	±	*0,7*
Vistula *	Poland	170,31	54.651	19.287	0,511903	±	11	-14,3	±	0,3
Neman **	Lithuania	90,32	55.3620	21.257	0,511905	±	7	-14,3	±	0,3
Daugava **	Latvia	90,44	57.060	24.039	0,511840	±	7	-15,5	±	0,3
Gauja *	Latvia	10,16	57.133	24.684	0,511911	±	7	-14,1	±	0,3
Narva**	Estonia	42,97	59.489	28.040	0,511795	±	11	-16,4	±	0,3
North European Plain - West & East (southern SIS)								*-13,4*	±	*1,9*
Scandinavia (inner SIS)								*-17,6*	±	*1,7*
Neva	Russia	211,90	60.070	29.279	0,511728	±	11	-17,7	±	0,3
Kymijoki *	Finland	54,32	60.260	26.496	0,511679	±	9	-18,7	±	0,3
Kiiminkijoki *	Finland	7,46	65.133	25.731	0,511443	±	11	-23,3	±	0,3
Luleälven	Sweden	53,53	65.682	21.820	0,511657	±	6	-19,1	±	0,3
Umeälven *	Sweden	50,75	63.718	20.267	0,511716	±	7	-17,9	±	0,3
Glomma *	Norway	59,90	59.929	11.162	0,511929	±	8	-13,8	±	0,3

*: data from Freslon et al. (2014)
**: data from Soulet et al. (2013)

Table3

Site location	ID	Country	Lat.	Long.	Sedimentary environments & Stratigraphy	Ref.	143Nd/144Nd	±	2se	εNd	±	2 sd
British Isles - Southern Ireland (ISIS)										*-8,7*	±	*4,6*
Whitting Bay East	WBE1	Ireland	51.949	-7.766	Muddy diamict (Irish Sea Till)	1	0.512078	±	7	-10,9	±	0,3
Ballycrooneen	BC1	Ireland	51.808	-8.114	Muddy diamict (Irish Sea Till)	1	0.512045	±	8	-11,5	±	0,3
Ardmore Bay	AB1	Ireland	51.973	-7.698	Muddy diamict (Irish Sea Till)	1	0.512040	±	9	-11,6	±	0,3
Kilmore Quay	KQE1	Ireland	52.167	-6.6	Muddy diamict (Irish Sea Till)	1	0.512604	±	14	-0,6	±	0,3
British Isles - Eastern Ireland (ISIS)										*-12,5*	±	*0,5*
Skerries	SK1	Ireland	53.58	-6.105	Muddy diamict (Irish Sea Till)	2	0.512022	±	7	-12,0	±	0,3
Killiney Bay	SPN1-2	Ireland	53.231	-6.108	Muddy diamict (Irish Sea Till)	3	0.511971	±	7	-13,0	±	0,3
British Isles - Southern & Eastern Ireland (ISIS)										*-11,8*	±	*0,7*
British Isles - East UK (BIIS)										*-13,1*	±	*0,8*
Happisburgh	HPB1	UK	52.826	1.533	Glaciolacustrine diamict (Anglian Stage)	4	0.511996	±	7	-12,5	±	0,3
Filey Bay	FLD1	UK	54.207	-0.284	Glaciolacustrine diamict (Filey Till, Filey lower Dms)	5	0.511903	±	5	-14,3	±	0,3
Filey Bay	FMD1	UK	54.207	-0.284	Glaciolacustrine diamict (Filey Till, Filey mid Dmm)	5	0.511994	±	6	-12,5	±	0,3
English Channel (downstream part of Channel River)										*-11,8*	±	*0,4*
English Channel	L1a-LV451	UK	50.643	0.098	Periglacial slope (terrestrial), north of the Channel River	6	0.512006	±	6	-12,3	±	0,3
English Channel	N4c-LV403	UK	50.608	0.113	Glaciofluvial (Northern Palaeovalley, Channel River)	6	0.512028	±	6	-11,9	±	0,3
English Channel	N4d-LV402	UK	50.608	0.114	Glaciofluvial (Northern Palaeovalley, Channel River)	6	0.512025	±	5	-11,9	±	0,3
Fosse Dangeard	CM02-03	France	51.015	1.479	Glaciolacustrine laminated silt	7	0.512068	±	7	-11,1	±	0,3
North Sea (confluence of BIIS and SIS)										*-12,2*	±	*1,5*
Dogger Bank	BGS1	UK	54.237	2.431	Glacimarine sediment (Dogger Bank Fm)	8	0.511983	±	5	-12,7	±	0,3
Dogger Bank	BGS3	UK	54.245	2.183	Glacimarine sediment (Dogger Bank Fm)	8	0.511966	±	6	-13,1	±	0,3
Dogger Bank	BGS6	UK	54.245	2.183	Glacimarine sediment (Dogger Bank Fm)	8	0.511953	±	6	-13,3	±	0,3
Dogger Bank	BGS11	UK	54.966	2.633	Glacimarine sediment (Dogger Bank Fm)	8	0.512140	±	9	-9,7	±	0,3
North European Plain - West (southwestern SIS)										*-14,8*	±	*1,3*
Knud Strand	KSS1	Denmark	56.658	8.777	Glaciolacustrine (Spøttrup, Fegge Clay)	9	0.511851	±	6	-15,3	±	0,3
Rubjerg Knude	LKFm1	Denmark	57.450	9.778	Glaciolacustrine (Lønstrup Klint Fm)	10	0.511777	±	6	-16,8	±	0,3
Rubjerg Knude	RKNFm1	Denmark	57.450	9.778	Glaciofluvial, outwash plain (Rubjerg Knude Fm)	10	0.511838	±	8	-15,6	±	0,3
Rubjerg Knude	RIBFm1	Denmark	57.450	9.778	Outwash plain (Ribjerg Fm)	10	0.511850	±	7	-15,3	±	0,3
Karup	KAR1	Denmark	56.312	9.185	Outwash plain (Karup Sandur Fm)	11	0.511969	±	6	-13,0	±	0,3
Travemünde	S1	Germany	53.971	10.883	Glaciolacustrine (Brodtener Ufer Cliff section)	12	0.512001	±	6	-12,4	±	0,3
Travemünde	S5	Germany	53.971	10.883	Glaciolacustrine (Brodtener Ufer Cliff section)	12	0.511910	±	5	-14,2	±	0,3
Beelitz	BEE-a	Germany	52.288	12.937	Outwash plain; Glogow-Baruth IMV (Brandenburg IMP)	13	0.511925	±	5	-13,9	±	0,3
Beelitz	BEE-b	Germany	52.288	12.937	Outwash plain; Glogow-Baruth IMV (Brandenburg IMP)	13	0.511929	±	6	-13,8	±	0,3
Althüttendorf	ALT-a	Germany	52.963	13.872	Outwash plain; Torun-Eberswalde IMV (Pomeranian IMP)	14	0.511790	±	6	-16,5	±	0,3
Althüttendorf	ALT-b	Germany	52.963	13.872	Outwash plain; Torun-Eberswalde IMV (Pomeranian IMP)	14	0.511830	±	5	-15,7	±	0,3
Macherslust	MAC-a	Germany	52.848	13.838	Glaciolacustrine; Torun-Eberswalde IMV (Pomeranian IMP)	14	0.511876	±	3	-14,8	±	0,3
Macherslust	MAC-b	Germany	52.848	13.838	Glaciolacustrine; Torun-Eberswalde IMV (Pomeranian IMP)	14	0.511837	±	5	-15,6	±	0,3
North European Plain - East (southeastern SIS)										*-15,1*	±	*0,8*
Wypaleniska	WP1.1	Poland	53.059	18.144	Vistula River erosional terrace (preceding the Leszno IA)	15	0.511884	±	6	-15,8	±	0,3
Wypaleniska	WP1.2	Poland	53.059	18.144	Vistula River erosional terrace (preceding the Leszno IA)	15	0.511913	±	6	-14,7	±	0,3
Trzciniec	TRZ	Poland	53.086	17.945	Outwash plain; Torun-Eberswalde IMV (Pomeranian IMP)	15	0.511913	±	6	-14,1	±	0,3
Gorzen	GRZ	Poland	53.133	17.729	River terrace; Torun-Eberswalde IMV (Pomeranian IMP)	15	0.511935	±	6	-13,7	±	0,3
Oborki	OBK	Poland	53.152	19.381	Till, till plain (Poznan IA)	16	0.511811	±	6	-16,1	±	0,3

Kozlowo	KZL	Poland	53.341	18.341	Till, till plain (Poznan IA)	17	0.511825	±	6	-15,8	±	0,3
Glaznoty	GLZ	Poland	53.535	19.904	Till, till plain (Poznan IA)	18	0.511827	±	6	-15,8	±	0,3
Chrostkowo	CHK1	Poland	52.943	19.253	Diamict, ice marginal belt (Poznan IMP)	19	0.511894	±	6	-14,5	±	0,3
Chrostkowo	CHK2	Poland	52.943	19.253	Diamict, ice marginal belt (Poznan IMP)	19	0.511855	±	6	-15,2	±	0,3
Karchowo	ST/12	Poland	51.889	16.834	Outwash plain; Glogow-Baruth IMV (Leszno IMP)	20	0.511820	±	4	-15,9	±	0,3
Karchowo	ST/13	Poland	51.889	16.834	Outwash plain; Glogow-Baruth IMV (Leszno IMP)	20	0.511888	±	8	-14,6	±	0,3
Karchowo	ST/14	Poland	51.889	16.834	Outwash plain; Glogow-Baruth IMV (Leszno IMP)	20	0.511844	±	4	-15,4	±	0,3
Hetmanice	ST/15	Poland	51.858	16.265	Outwash plain; Glogow-Baruth IMV (Leszno IMP)	20	0.511921	±	6	-13,9	±	0,3
Hetmanice	ST/16	Poland	51.858	16.265	Outwash plain; Glogow-Baruth IMV (Leszno IMP)	20	0.511792	±	4	-16,5	±	0,3
Hetmanice	ST/17	Poland	51.858	16.265	Outwash plain; Glogow-Baruth IMV (Leszno IMP)	20	0.511874	±	5	-14,9	±	0,3
North European Plain - West & East (southern SIS)										*-15,0*	±	*1,1*

Table4

Channel River Runoff Events (R)	start date (cal ka BP)	end date (cal ka BP)	SIS Dynamic	North Atlantic / Greenland Climate Event
	16.7 ± 0.2 [a]	15.7 ± 0.3 [b]	Pomeranian ice advance	HS1 (second part = HE1)
R5	18.2 ± 0.2	16.7 ± 0.2	(subtantial) ice marginal retreat	HS1 (first part)
	18.7 ± 0.3	18.2 ± 0.2	Frankfurt-Poznan ice advance	-
R4	20.3 ± 0.2	18.7 ± 0.3	(significant) ice marginal retreat	19-ky MWP [c]
	21.3 ± 0.2	20.3 ± 0.2	(Late) Brandenburg-Leszno ice advance	-
R3	22.5 ± 0.2	21.3 ± 0.2	(moderate) ice marginal retreat (onset deglaciation)	-
	23.4 ± 0.3	22.5 ± 0.5	(Early) Brandenburg-Leszno ice advance (LGM)	-
R2	25.7 ± 0.3	23.4 ± 0.3	(moderate) ice marginal retreat	HS2
	28.9 ± 0.4	25.7 ± 0.3	ice advance (to LGM position) [d]	GI3-GI4
R1	30.7 ± 0.7	28.9 ± 0.4	(moderate) ice marginal retreat	HS3
	~ 35 [e]	30.7 ± 0.7	ice advance (onset Weichselian glaciation) e	GI5-GI6 [f]

a : this study; 17.2 ± 0.4 ka in Soulet et al. (2013)

b : Soulet et al. (2013) in good agreement with new exposure ages (Rinterknecht et al., 2012, 2013)

c : Carlson et Clark (2012), Clark et al. (2004), Yokoyama et al. (2000)

d: see Houmark-Nielsen (2003; Kattegat ice advance, Denmark) and Bradwell et al. (2008; North Sea)

e : see Bradwell et al. (2008; North Sea), Houmark-Nielsen et al. (2010; Klintholm ice advance, Denmark), Mangerud et al. (2010; Rogne Stadial, western Norway) and Marks (2012; late Middle Vistulian, Poland) among others

f : see Mangerud et al. (2010)

Figure1

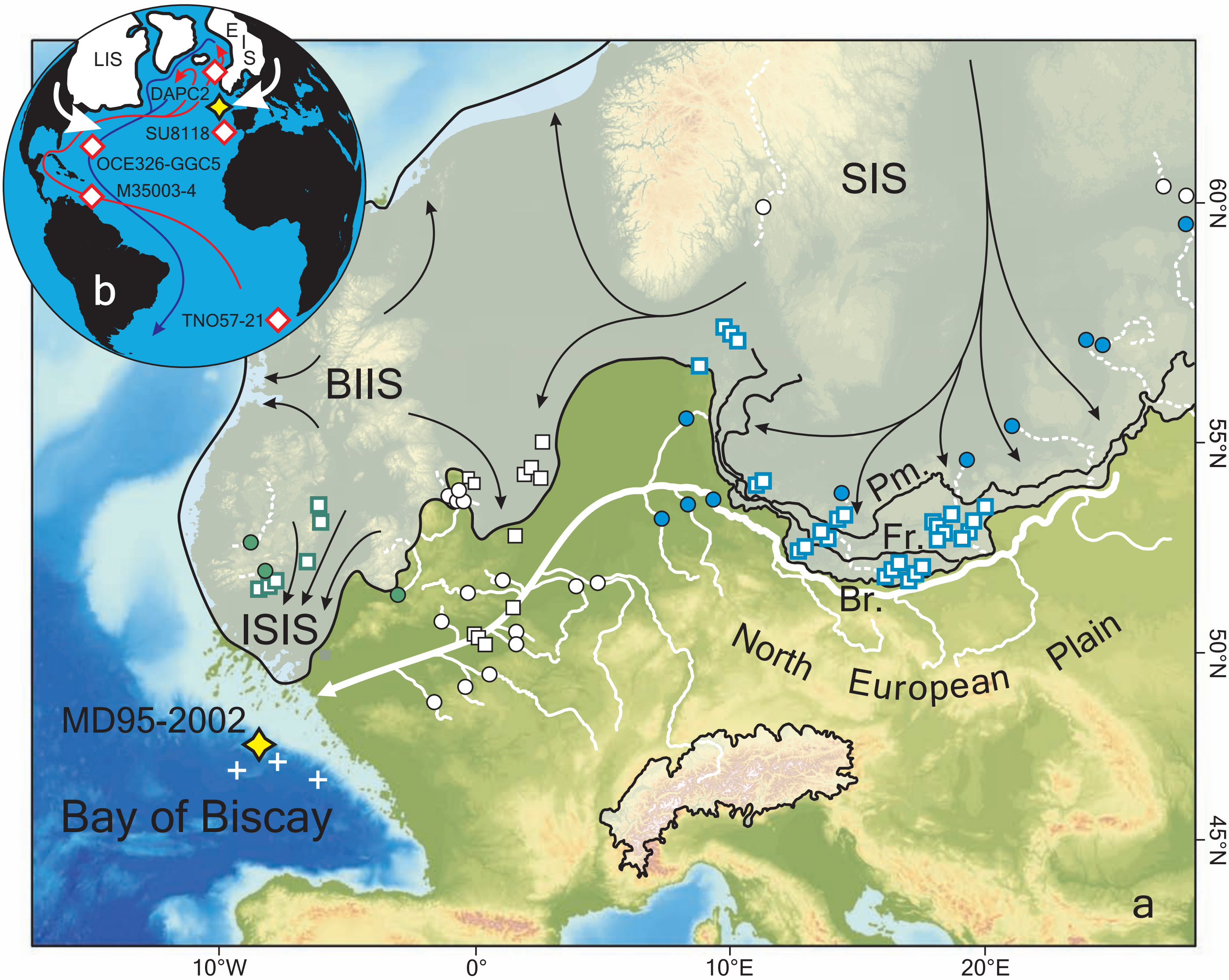

LIS
E
I
S
DAPC2
SU8118
OCE326-GGC5
M35003-4
TNO57-21
b
SIS
BIIS
ISIS
Pm.
Fr.
Br.
North European Plain
MD95-2002
Bay of Biscay
a
60°N
55°N
50°N
45°N
10°W
0°
10°E
20°E

Figure2

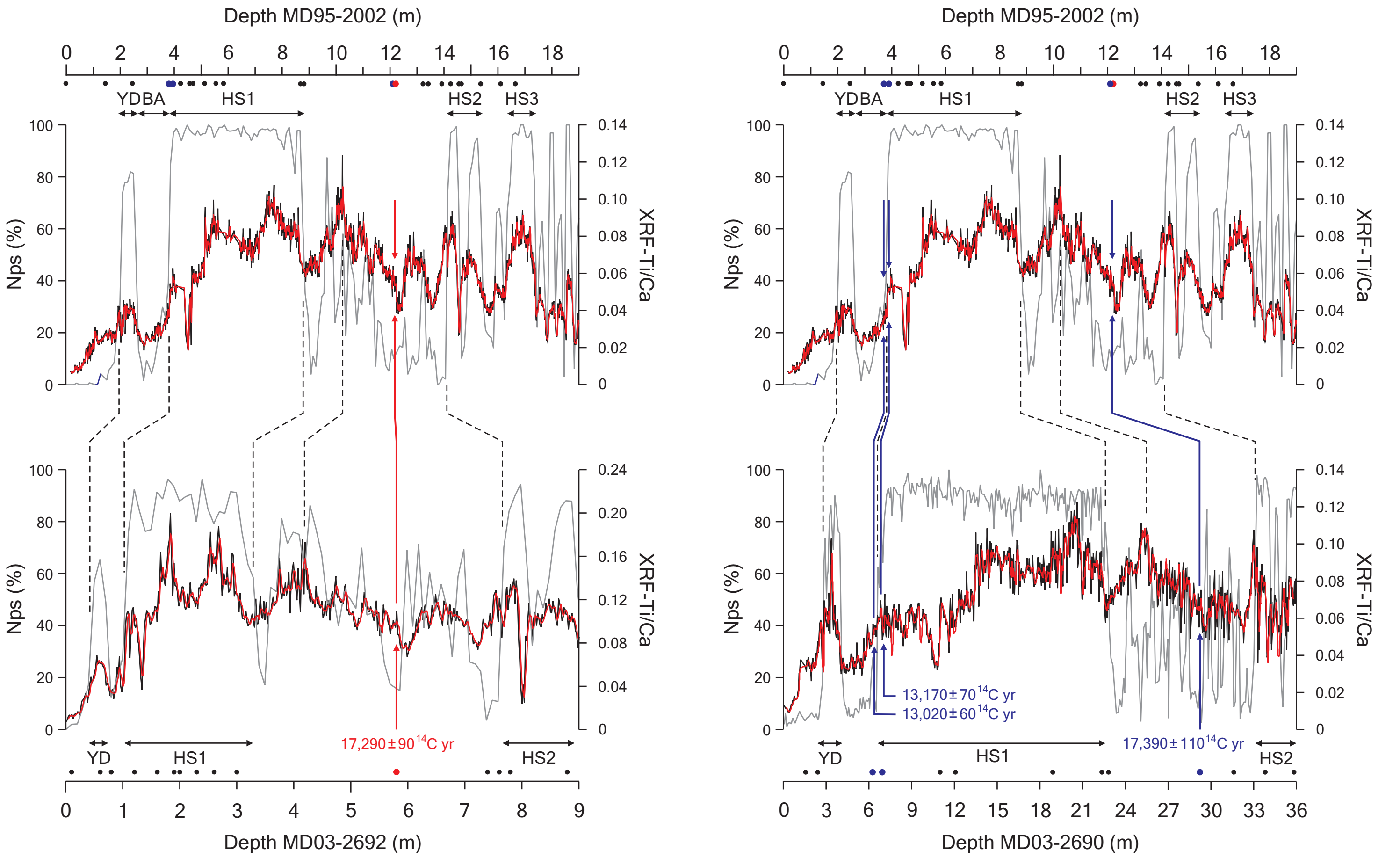

Depth MD95-2002 (m)
YD
BA
HS1
HS2
HS3
Nps (%)
XRF-Ti/Ca
17,290±90 ¹⁴C yr
Depth MD03-2692 (m)
13,170±70 ¹⁴C yr
13,020±60 ¹⁴C yr
17,390±110 ¹⁴C yr
Depth MD03-2690 (m)

Figure3

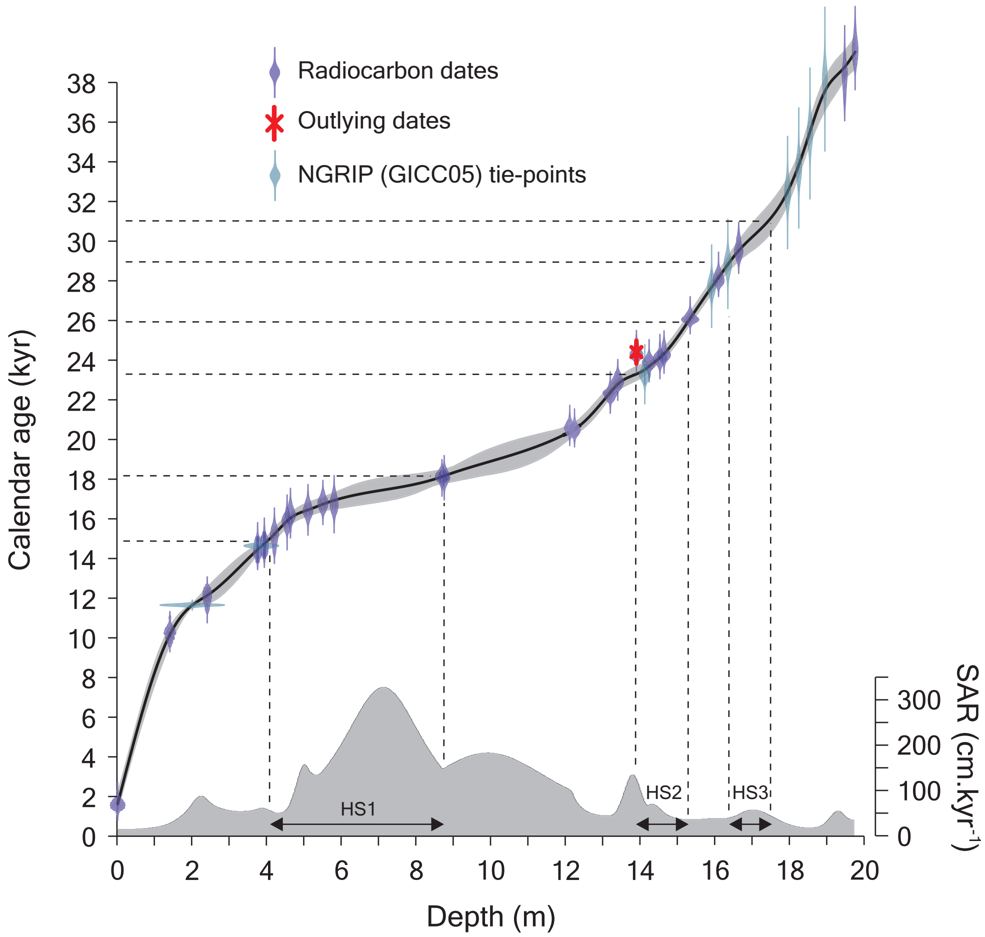

Radiocarbon dates
Outlying dates
NGRIP (GICC05) tie-points
Calendar age (kyr)
Depth (m)
SAR (cm.kyr-1)
HS1
HS2
HS3
0
2
4
6
8
10
12
14
16
18
20
22
24
26
28
30
32
34
36
38
100
200
300

Figure4

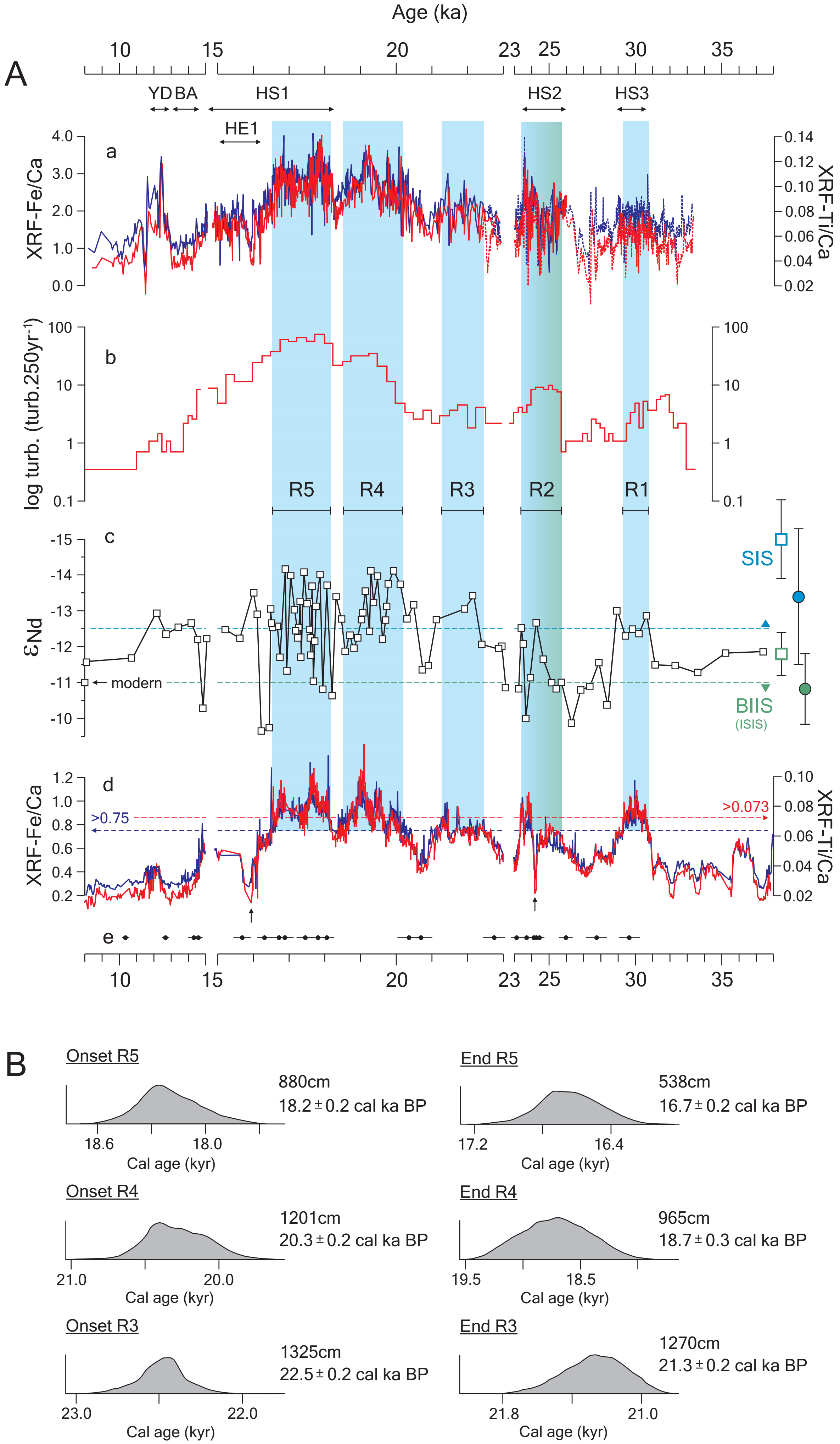

A
Age (ka)
YD BA HS1 HS2 HS3
HE1
XRF-Fe/Ca
XRF-Ti/Ca
log turb. (turb.250yr⁻¹)
R5 R4 R3 R2 R1
εNd
modern
SIS
BIIS
(ISIS)
>0.75
>0.073
B
Onset R5
880cm
18.2 ± 0.2 cal ka BP
End R5
538cm
16.7 ± 0.2 cal ka BP
Onset R4
1201cm
20.3 ± 0.2 cal ka BP
End R4
965cm
18.7 ± 0.3 cal ka BP
Onset R3
1325cm
22.5 ± 0.2 cal ka BP
End R3
1270cm
21.3 ± 0.2 cal ka BP
Cal age (kyr)

Figure5

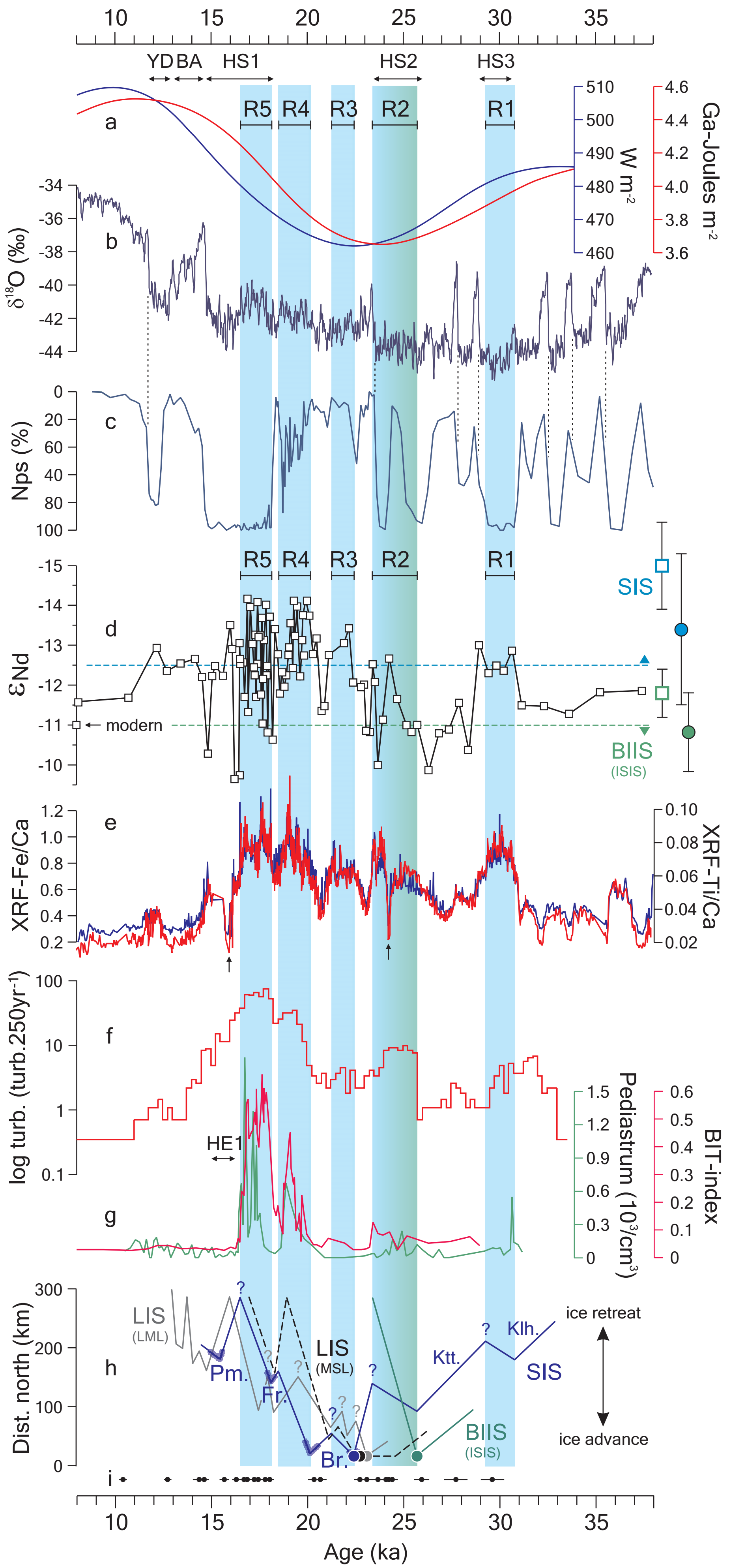

YD
BA
HS1
HS2
HS3
R5
R4
R3
R2
R1
a
b
c
d
e
f
g
h
i
W m-2
Ga-Joules m-2
δ18O (‰)
Nps (%)
εNd
modern
SIS
BIIS
(ISIS)
XRF-Fe/Ca
XRF-Ti/Ca
log turb. (turb.250yr-1)
HE1
Pediastrum (10³/cm³)
BIT-index
Dist. north (km)
LIS
(LML)
LIS
(MSL)
Pm.
Fr.
Br.
Ktt.
Klh.
SIS
BIIS
(ISIS)
ice retreat
ice advance
Age (ka)

Figure6

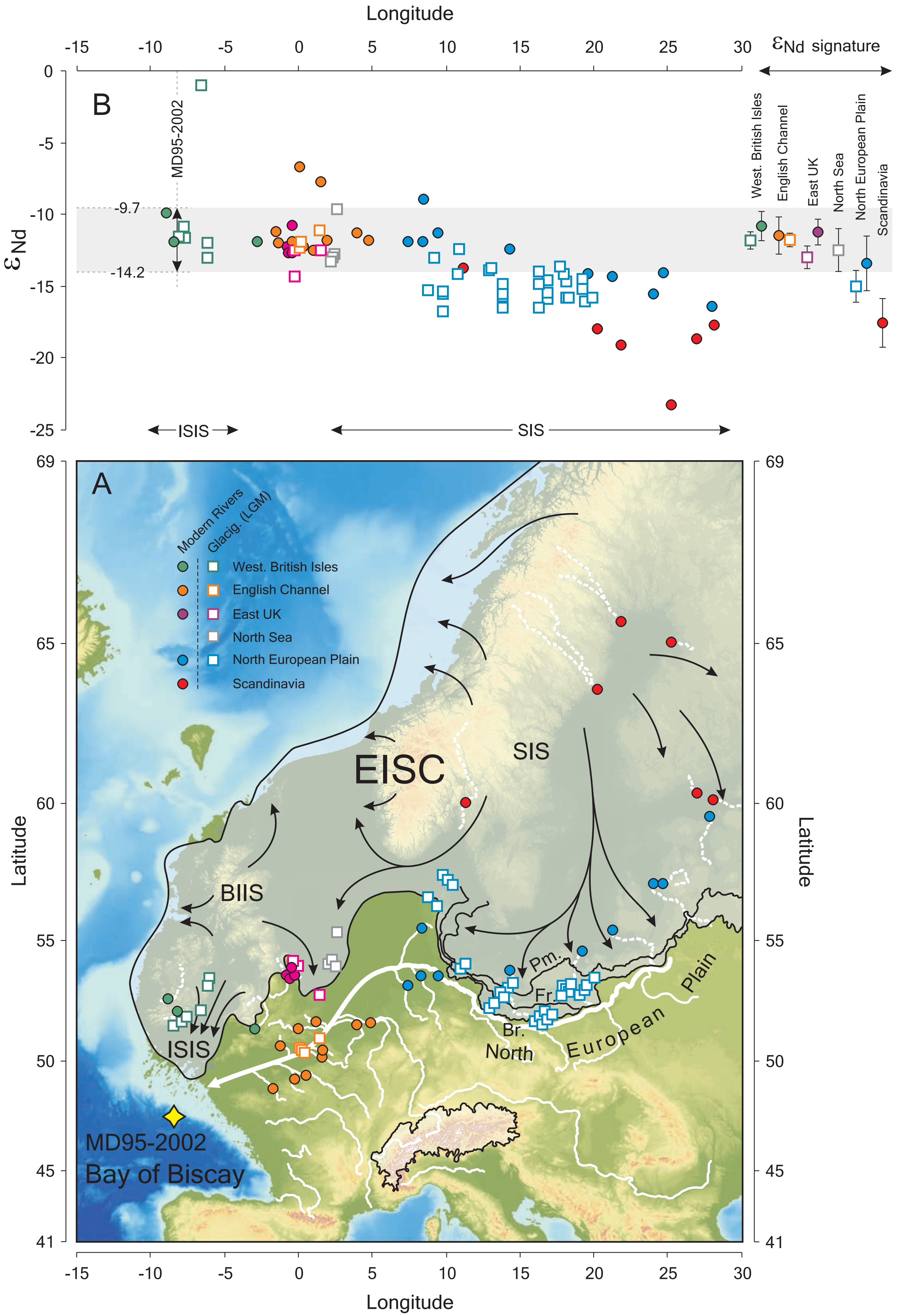
Longitude
εNd signature
B
MD95-2002
-9.7
-14.2
εNd
West. British Isles
English Channel
East UK
North Sea
North European Plain
Scandinavia
ISIS
SIS
A
Modern Rivers
Glacig. (LGM)
West. British Isles
English Channel
East UK
North Sea
North European Plain
Scandinavia
EISC
SIS
BIIS
ISIS
Pm.
Fr.
Br.
North European Plain
MD95-2002
Bay of Biscay
Latitude
Longitude

Figure7

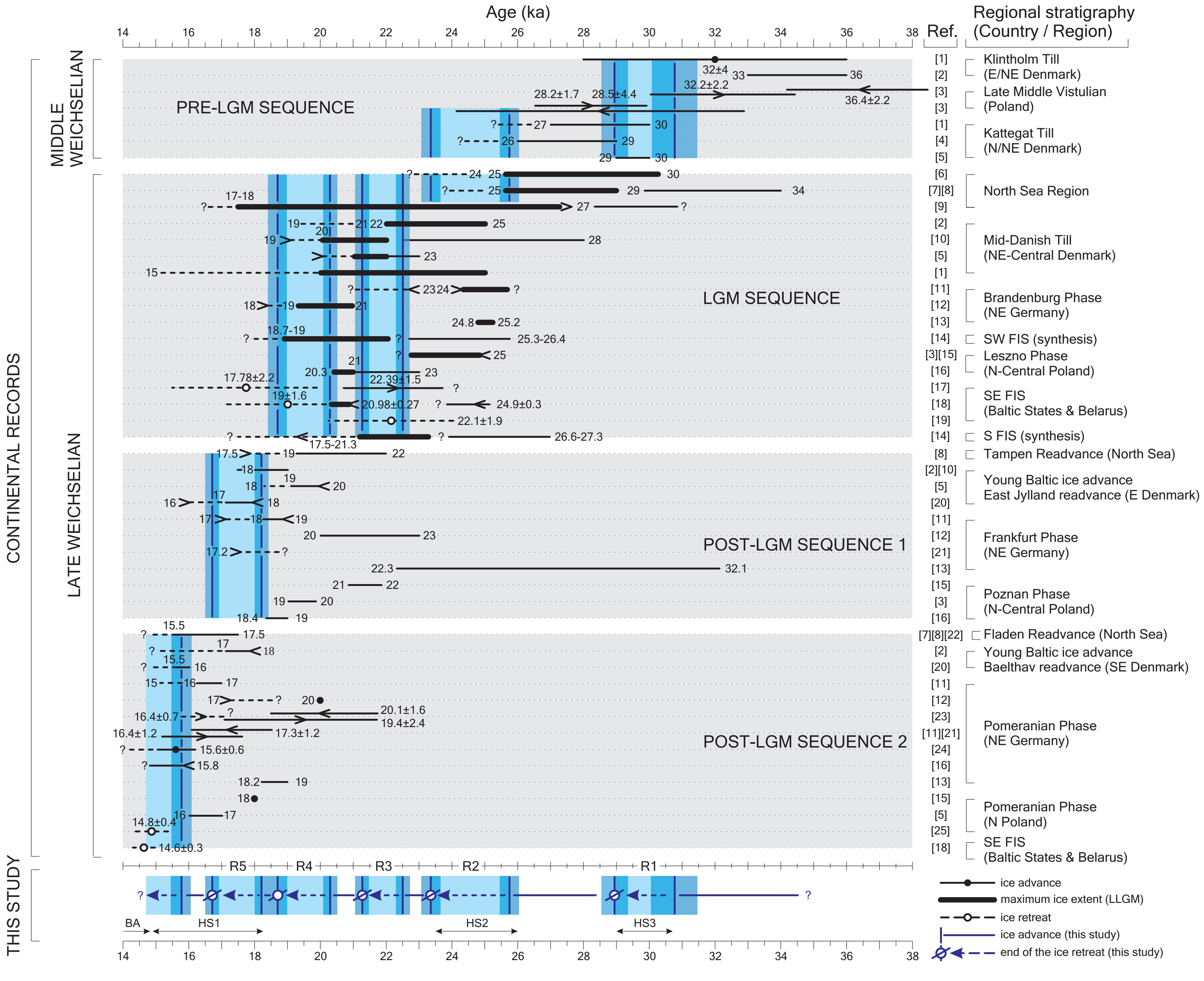

Age (ka)
Ref.
Regional stratigraphy (Country / Region)
MIDDLE WEICHSELIAN
LATE WEICHSELIAN
CONTINENTAL RECORDS
THIS STUDY
PRE-LGM SEQUENCE
LGM SEQUENCE
POST-LGM SEQUENCE 1
POST-LGM SEQUENCE 2
Klintholm Till (E/NE Denmark)
Late Middle Vistulian (Poland)
Kattegat Till (N/NE Denmark)
North Sea Region
Mid-Danish Till (NE-Central Denmark)
Brandenburg Phase (NE Germany)
SW FIS (synthesis)
Leszno Phase (N-Central Poland)
SE FIS (Baltic States & Belarus)
S FIS (synthesis)
Tampen Readvance (North Sea)
Young Baltic ice advance East Jylland readvance (E Denmark)
Frankfurt Phase (NE Germany)
Poznan Phase (N-Central Poland)
Fladen Readvance (North Sea)
Young Baltic ice advance Baelthav readvance (SE Denmark)
Pomeranian Phase (NE Germany)
Pomeranian Phase (N Poland)
SE FIS (Baltic States & Belarus)
R5
R4
R3
R2
R1
BA
HS1
HS2
HS3
ice advance
maximum ice extent (LLGM)
ice retreat
ice advance (this study)
end of the ice retreat (this study)

Figure8

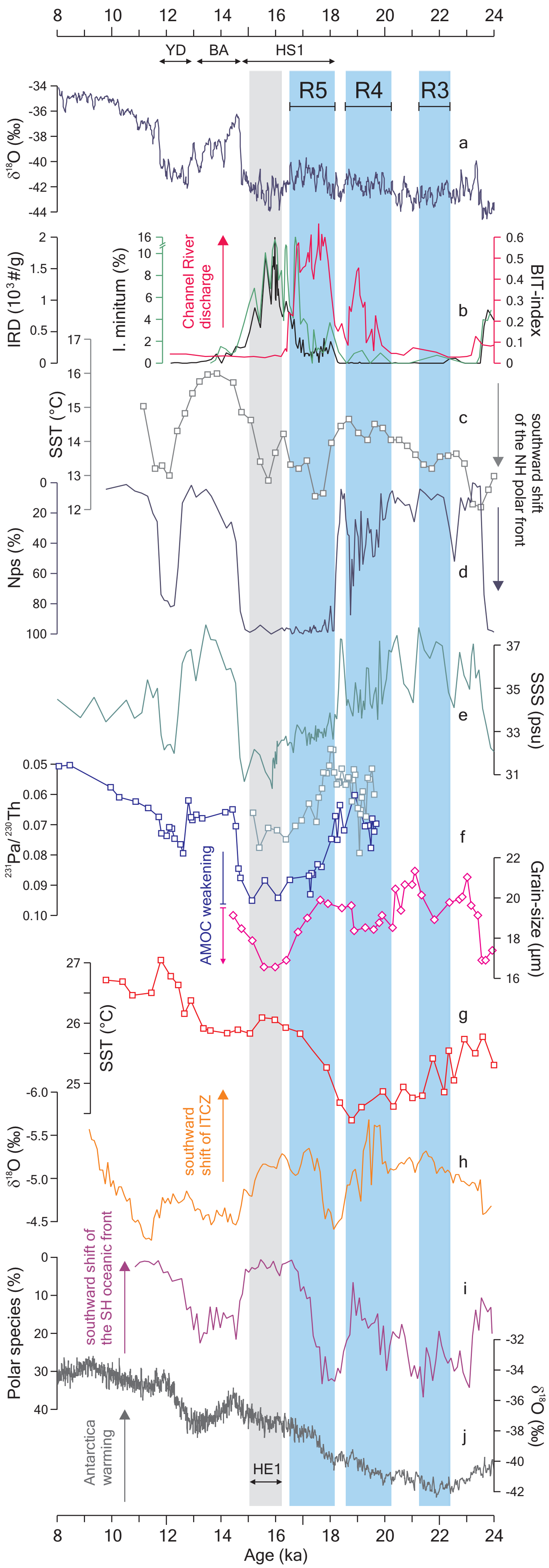

YD
BA
HS1
R5
R4
R3
HE1
δ18O (‰)
IRD (10³ #/g)
I. minitum (%)
Channel River discharge
BIT-index
SST (°C)
southward shift of the NH polar front
Nps (%)
SSS (psu)
231Pa/230Th
AMOC weakening
Grain-size (μm)
SST (°C)
δ18O (‰)
southward shift of ITCZ
Polar species (%)
southward shift of the SH oceanic front
Antarctica warming
δ18O (‰)
a
b
c
d
e
f
g
h
i
j
Age (ka)

Supplementary Data

Click here to download Supplementary Data: SupplMaterial.pdf